

# Effective Permeability of a Porous Medium with Spherical and Spheroidal Vug and Fracture Inclusions

Mojdeh Rasoulzadeh<sup>1</sup> · Fikri J. Kuchuk<sup>1</sup>

Received: 1 February 2016 / Accepted: 1 November 2016 / Published online: 25 November 2016  
© Springer Science+Business Media Dordrecht 2016

**Abstract** Vugs and fractures are common features of carbonate formations. The presence of vugs and fractures in porous media can significantly affect pressure and flow behavior of a fluid. A vug is a cavity (usually a void space, occasionally filled with sediments), and its pore volume is much larger than the intergranular pore volume. Fractures occur in almost all geological formations to some extent. The fluid flow in vugs and fractures at the microscopic level does not obey Darcy's law; rather, it is governed by Stokes flow (sometimes is also called Stokes' law). In this paper, analytical solutions are derived for the fluid flow in porous media with spherical- and spheroidal-shaped vug and/or fracture inclusions. The coupling of Stokes flow and Darcy's law is implemented through a no-jump condition on normal velocities, a jump condition on pressures, and generalized Beavers–Joseph–Saffman condition on the interface of the matrix and vug or fracture. The spheroidal geometry is used because of its flexibility to represent many different geometrical shapes. A spheroid reduces to a sphere when the focal length of the spheroid approaches zero. A prolate spheroid degenerates to a long rod to represent the connected vug geometry (a tunnel geometry) when the focal length of the spheroid approaches infinity. An oblate spheroid degenerates to a flat spheroidal disk to represent the fracture geometry. Once the pressure field in a single vug or fracture and in the matrix domains is obtained, the equivalent permeability of the vug with the matrix or the fracture with matrix can be determined. Using the effective medium theory, the effective permeability of the vug–matrix or fracture–matrix ensemble domain can be determined. The effect of the volume fraction and geometrical properties of vugs, such as the aspect ratio and spatial distribution, in the matrix is also investigated. It is shown that the higher volume fraction of the vugs or fractures enhances the effective permeability of the system. For a fixed-volume fraction, highly elongated vugs or fractures significantly increase the effective permeability compared with shorter vugs or fractures. A set of disconnected vugs or fractures yields lower effective permeability compared with a single vug or fracture of the same volume fraction.

---

✉ Fikri J. Kuchuk  
kuchuk1@slb.com

<sup>1</sup> Schlumberger-Doll Research, MD#A353, One Hampshire Street, Cambridge, MA 02139-1578, USA

## Nomenclature

$a$	Major semi-axis of spheroid
$b$	Minor semi-axis of spheroid
$c$	Confocal distance
$\mathbf{e}_{1,2,3}$	Normal unit vectors of the curvilinear coordinate system
$\epsilon$	Rate of strain tensor
$G_n$	Gegenbauer function of first kind
$\Gamma_{p,v}$	Interface of porous and vuggy domain
$h_{1,2,3}$	Scale factors of curvilinear coordinate system
$H_n$	Gegenbauer function of second kind
$\eta$	Spheroidal coordinate
$k$	Permeability
$\lambda$	Beavers–Joseph–Saffman empirical coefficient
$\mu$	Fluid viscosity
$\mathbf{n}$	Unit normal vector to the interface
$Q_n$	Legendre polynomial of second kind and order $n$
$p$	Pressure
$P_n$	Legendre polynomial of first kind and order $n$
$\phi$	Spheroidal coordinate
$\psi$	Streamline
$r$	Distance from the origin
$\rho$	Fluid density and spherical coordinate
$s$	Spheroidal coordinate
$\boldsymbol{\tau}$	Unit tangential vector to the interface
$t$	Spheroidal coordinate
$U_\infty$	Constant velocity field at the infinity
$u$	Velocity element
$\mathbf{u}$	Velocity vector
$v$	Velocity element
$x$	Cartesian coordinate
$\xi$	Spheroidal coordinate
$\chi$	Curvilinear coordinate
$x$	Dummy variable
$y$	Cartesian coordinate
$z$	Cartesian coordinate
$\Omega_m$	Porous matrix
$\Omega_v$	Vug domain

## Subscripts

m	Parameter in matrix
v	Parameter in vug
in	Parameter in porous inclusion
s	Parameter for spherical shape of vug or inclusion

## 1 Introduction

Carbonate formations, particularly naturally fractured ones, usually have connected and nonconnected fractures, matrix (host porous media of inclusions), and connected and non-connected vugs. A vug is a cavity, inclusion, or void pore, which is larger compared with the intergranular pore size, and created by rock dissolution (diagenesis). Vugs normally have almost infinite permeability and are normally elongated in one direction in the horizontal plane. Some vugs can have irregular shapes, but can still be roughly approximated by spheroids. As shown in Fig. 1, several vugs can be connected with each other, referred to as touching vugs (Lucia 1999), and create wormholes without many branches. Fractures are mechanical breaks in rocks and create discontinuities with a displacement across surfaces or narrow zones (Committee on Fracture Characterization and Fluid Flow 1996). Unlike vugs, fractures normally have planar shapes, with much smaller apertures than their vertical height and lateral length. Connected vugs are created by further rock dissolution and fracturing and can also be enlarged by additional dissolution.

Here, we focus on microfractures, and short (less than a few tens of meters) secondary and tertiary fractures, which are assumed to be discrete or only locally continuous and not continuous or discrete primary (major) fractures or any long fractures (more than a few tens of meters). Fractures and vugs are embedded in the matrix; thus, they contribute to the effective matrix permeability and porosity. If vugs and/or secondary and tertiary open fractures are directly connected to the major fractures, then they must be a part of the fracture system, for which Kuchuk et al. (2015) presented the modeling details of such fracture systems.

In most carbonate formations, vug sizes vary from a few  $\mu\text{m}$  to thousands of  $\mu\text{m}$  (Arns et al. 2005), while fracture apertures vary from 0.001 to 10 mm (Bertels et al. 2001; Detwiler et al. 2001; Keller et al. 1999). Thus, fracture-intersecting vugs do not make any observable change in the fracture conductivity, although they may enhance fracture conductivities for low-conductivity fractures. Naturally fractured formations might contain many faults and thousands of fractures with different apertures, conductivities, lengths, orientations, sizes, and spacings and may well have a power-law distribution of these properties (Aarseth et al. 1997; Belfield and Sovich 1994; Braester 2005; Nurmi et al. 1995). This condition implies that naturally fractured formations might contain hundreds or thousands of primary fractures, and possibly thousands or millions of small vertical and near-vertical fractures. Consequently,

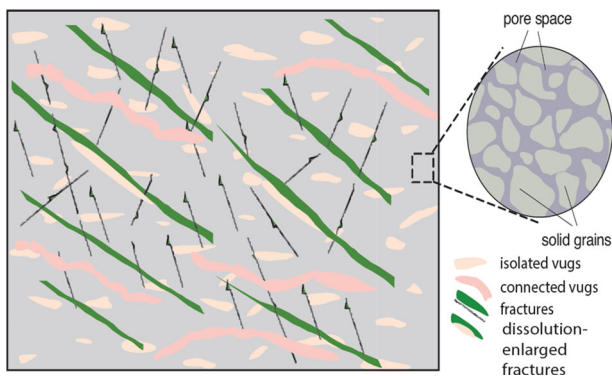


**Fig. 1** Connected and isolated vugs, and fractures

it is important to obtain the effective permeability of the matrix with thousands or millions small discrete and/or only locally continuous fractures.

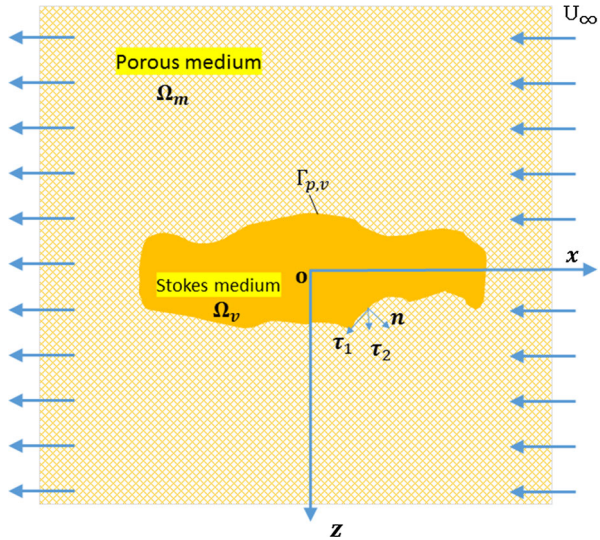
In this paper, we deal with four possible vug/fracture systems: isolated vugs, connected vugs, fractures, and dissolution-enlarged fractures, as shown in Fig. 1. For a given rock volume, all or any combination of these vug/fracture systems might occur. Although the geometry of the majority of vugs can be described by a spherical shape, a wide range of vugs have elongated shapes, which cannot be described by a spherical shape. Spheroidal shapes (axis-symmetric ellipsoids) are very suitable choices for describing a variety of vug geometries. These shapes can cover geometries with an aspect ratio close to 1, spherical geometry, as well as elongated, needle-like shapes with a large aspect ratio. Isolated vugs will be treated as being spherical or spheroidal in shape, whereas vugs will be treated as elongated spheroidal shapes and fractures will be treated as vertical spheroidal disks. Therefore, the spheroidal geometry will provide us sufficient flexibility to work with a wide variety of vugs and fracture shapes. A spheroid is reduced to a sphere when the focal length of the spheroid approaches zero. A prolate spheroid degenerates to a long rod when the focal length of the spheroid approaches infinity, and it represents the connected vug geometry (a tunnel geometry). An oblate spheroid degenerates to a flat spheroidal disk that can approximate the fracture geometry. We use the term vug to address both vug and microfracture inclusions.

The spatial resolution of petrophysical logs and cores is still very limited for a good quality description of vuggy and fractured media. Standard sampling methods such as thin sections, core plugs, and even whole core are perhaps, for most cases, too small to measure the effective permeability of a vuggy and/or fractured medium. In particular, the standard Hassler core plugs are too small to measure the effective permeability.

Mostly numerical methods have been widely used to investigate fluid flow in porous media with vugs (Arbogast and Brunson 2007; Arbogast et al. 2004; Arbogast and Gomez 2009; Moctezuma-Berthier et al. 2002, 2004; Wieck et al. 1995; Zhao and Valliappan 1994), where a coupled system of equations of flow including Stokes flow (Stokes' law) in the vugs and Darcy's law in the matrix is solved by use of finite element or finite volume method. Asymptotic solution to this problem through the homogenization technique was obtained for the case of binary medium where a vug is periodically repeated through the porous matrix (Arbogast and Lehr 2006; Bouchelaghem 2011a, b). At the fine scale, the Stokes flow in the vug was coupled to the Darcy's law in the matrix. A macroscopic Darcy's law governing fluid flow in the macroscale porous medium was obtained. The cell problem, resulting in the macroscale effective permeability, was solved numerically for several vug shapes by Arbogast and Lehr (2006). Analytical solutions for the cell problem of a similar case for spheroidal vugs was obtained by Bouchelaghem (2011a, b). Another similar upscaling approach was presented by Popov et al. (2009) in which the Stokes–Brinkman equation rather than the Darcy–Stokes equation was used at the fine scale to compute the upscaled effective permeability of fractured karst carbonate reservoirs based on homogenization theory. The Stokes–Brinkman equations can be reduced to either the Stokes or the Darcy equations by appropriate choice of parameters to avoid the explicit formulation of the boundary conditions at the fluid–matrix interfaces.

The exact analytical solution for fluid flow in porous media including a single circular or slightly deformed circular-shaped vug was obtained by Raja Sekhar and Sano (2000) and Raja Sekhar and Sano (2003). Markov et al. (2010) developed an analytical solution for the fluid flow and effective permeability of a vuggy porous media, including circular and spherical vugs. Happel and Brenner (1983), using the separation of variables method, obtained for the first time an analytical solution for Stokes flow past a spheroidal vugs. Fitts (1991) obtained

**Fig. 2** Schematic of the fluid flow through a vuggy inclusion located at the center of the matrix cell



an analytical solution for fluid flow in the vuggy porous domain containing porous inclusions in the shape of prolate or oblate spheroids.

The objective of this paper is to derive the effective permeability of a porous medium, including spherical- and/or spheroidal-shaped vug and/or fracture inclusions. For this purpose, an incompressible, steady-state, single-phase Darcian flow in the matrix medium is coupled with Stokes flow inside the spheroidal vug. Then, analytic solutions for the Stokes flow inside the spheroid are derived as a set of semi-separable solutions in terms of the ellipsoidal coordinates (Charalambopoulos and Dassios 2002; Dassios 2007; Dassios et al. 1994, 2004; Iyengar and Radhika 2011, 2015; Radhika and Iyengar 2010). The fluid flow field in the matrix medium is coupled with the Stokes flow in the vug through a no-jump condition on normal velocities, jump on pressures, and the generalized Beavers–Joseph–Saffman condition given by Beavers and Joseph (1967) and Jones (1973) on the matrix and vug or fracture interface. The equivalent permeability of the vug or fracture is obtained by substituting it with a porous vug having the same external matrix pressure field. The effective permeability of the ensemble of the system is obtained by using the volume averaging of the pressure field and velocity over the domain (Rubin and Gómez-Hernández 1990). The effect of shape, spatial distribution, and volume concentration of vugs on the effective permeability is investigated.

## 2 Mathematical Formulation of the Problem

A steady-state axis-symmetric flow of an incompressible fluid is assumed in a porous medium, in which the fluid-filled vuggy inclusions of different sizes and shapes are scattered throughout. The matrix domain is exposed to an external uniform pressure gradient. The size of a matrix cell is assumed to be sufficiently large compared with the vug size; therefore, in the far field the pressure field remains unaffected by the presence of vuggy inclusions. We begin our analysis with the case of only one vuggy inclusion,  $\Omega_v$ , located at the center of a relatively large matrix cell  $\Omega_m$  as shown in Fig. 2. The origin of the coordinate system is located at the center of the vug. The external uniform pressure gradient is assumed to be in the  $x$  direction of the elongated axis of the vug, denoted by the Cartesian coordinates  $(x, y, z)$ .

In the matrix domain, the conservation of mass and Darcy’s law can be expressed as

$$\nabla \cdot \mathbf{u}_m = 0, \quad \text{in } \Omega_m, \tag{1}$$

$$\mathbf{u}_m = -\frac{k_m}{\mu} \nabla p_m, \quad \text{in } \Omega_m, \tag{2}$$

where  $\mathbf{u}_m = (u_m, v_m)$ ,  $p_m$ ,  $k_m$ , and  $\mu$  denote the velocity vector, the pressure, the permeability, and the fluid viscosity in the matrix domain, respectively. In general, the subscript  $m$  refers to the matrix domain variables and properties. The fluid is assumed to be the same in the matrix and vuggy domains. The pressure field for the matrix domain from Eqs. 1 and 2 can be written as

$$\nabla^2 p_m = 0, \quad \text{in } \Omega_m. \tag{3}$$

In a general orthogonal curvilinear coordinate system  $(\chi_1, \chi_2, \chi_3)$  with  $(\mathbf{e}_{\chi_1}, \mathbf{e}_{\chi_2}, \mathbf{e}_{\chi_3})$  as the base vectors and  $(h_1, h_2, h_3)$  as the corresponding scale factors, the del and Laplacian operator are as follows

$$\nabla = \frac{1}{h_1} \frac{\partial}{\partial \chi_1} \mathbf{e}_{\chi_1} + \frac{1}{h_2} \frac{\partial}{\partial \chi_2} \mathbf{e}_{\chi_2} + \frac{1}{h_3} \frac{\partial}{\partial \chi_3} \mathbf{e}_{\chi_3}, \tag{4}$$

$$\nabla^2 = \frac{1}{h_1 h_2 h_3} \left[ \frac{\partial}{\partial \chi_1} \left( \frac{h_2 h_3}{h_1} \frac{\partial}{\partial \chi_1} \right) + \frac{\partial}{\partial \chi_2} \left( \frac{h_1 h_3}{h_2} \frac{\partial}{\partial \chi_2} \right) \right]. \tag{5}$$

For the axis-symmetric fluid flow, where  $\frac{\partial}{\partial \chi_3} = 0$ , the stream function  $\Psi_m$  in the matrix domain is introduced as

$$\begin{aligned} u_m &= \frac{1}{h_2 h_3} \frac{\partial \Psi_m}{\partial \chi_2}, \quad \text{in } \Omega_m, \\ v_m &= -\frac{1}{h_1 h_3} \frac{\partial \Psi_m}{\partial \chi_1}, \quad \text{in } \Omega_m. \end{aligned} \tag{6}$$

Inside the vug, the fluid flow is assumed to be laminar and happening at small Reynolds number with negligible inertial forces. This means that Stokes flow takes place inside the vug, for which the steady-state mass and momentum balance equations can be written as

$$\nabla \cdot \mathbf{u}_v = 0, \quad \text{in } \Omega_v, \tag{7}$$

$$\nabla p_v + \mu \nabla \times \nabla \times \mathbf{u}_v = 0, \quad \text{in } \Omega_v, \tag{8}$$

where,  $\mathbf{u}_v = (u_v, v_v)$  and  $p_v$  denote the velocity vector and the pressure inside the vug inclusion, respectively. We introduce the stream function  $\Psi_v$  inside the vug as

$$\begin{aligned} u_v &= \frac{1}{h_2 h_3} \frac{\partial \Psi_v}{\partial \chi_2}, \quad \text{in } \Omega_v, \\ v_v &= -\frac{1}{h_1 h_3} \frac{\partial \Psi_v}{\partial \chi_1}, \quad \text{in } \Omega_v. \end{aligned} \tag{9}$$

Obtaining the curl of Eq. 8, together with some mathematical manipulations, the stream function in the Stokes domain satisfies the following equation

$$E^4 \Psi_v = E^2 (E^2 \Psi_v) = 0, \quad \text{in } \Omega_v, \tag{10}$$

where the differential operator  $E^2$  is given by

$$E^2 = \frac{h_3}{h_1 h_2} \left[ \frac{\partial}{\partial \chi_1} \left( \frac{h_2}{h_1 h_3} \frac{\partial}{\partial \chi_1} \right) + \frac{\partial}{\partial \chi_2} \left( \frac{h_1}{h_2 h_3} \frac{\partial}{\partial \chi_2} \right) \right]. \tag{11}$$

Using this notation, Eq. 8 can be written as

$$\begin{aligned}
 -\frac{1}{h_1} \frac{\partial p_v}{\partial \chi_1} + \frac{\mu}{h_2 h_3} \frac{\partial}{\partial \chi_2} (E^2 \Psi_v) &= 0, \quad \text{in } \Omega_v, \\
 -\frac{1}{h_2} \frac{\partial p_v}{\partial \chi_2} - \frac{\mu}{h_1 h_3} \frac{\partial}{\partial \chi_1} (E^2 \Psi_v) &= 0, \quad \text{in } \Omega_v.
 \end{aligned}
 \tag{12}$$

In the orthogonal curvilinear coordinate system, the differential operators  $\nabla^2$  and  $E^2$  remain separable with respect to the spatial coordinates. The problem is closed with the following set of regularity conditions and the boundary condition on the interface of the vug and matrix domains.

*Bounded Velocity Inside the Vug*

$$\lim_{r \rightarrow 0} |\Psi_v(\chi_1, \chi_2, \chi_3)| < \infty, \tag{13}$$

$$\lim_{r \rightarrow 0} |u_v| < \infty, \quad \lim_{r \rightarrow 0} |v_v| < \infty, \tag{14}$$

where  $r$  is the distance of any point inside the vug from the origin of coordinate system.

*Regularity of Pressure Field at Infinity*

$$\lim_{x \rightarrow \infty} p_m = |\nabla(p_m)_\infty| x. \tag{15}$$

$\nabla(p_m)_\infty$  is the uniform pressure gradient in the matrix in  $x$ -direction at infinity and is not perturbed due to presence of the inclusion.

*Continuity of the Normal Velocities on the Interface* This condition guarantees the conservation of mass between porous matrix and the vug.

$$\mathbf{u}_v \cdot \mathbf{n} = \mathbf{u}_m \cdot \mathbf{n}, \quad \text{on } \Gamma_{m,v}, \tag{16}$$

where  $\mathbf{n}$  is the unit normal to the interface and  $\Gamma_{m,v}$  is the interface of the matrix cell and the vug as shown in Fig. 2.

*Pressure Jump on the Interface* This condition represents the balance of two driving forces in the normal direction along the interface, the kinematic pressure in the matrix and the normal component of the normal stress in the vug.

$$-p_m = -p_v + 2\mu \mathbf{n} \cdot \boldsymbol{\epsilon} \cdot \mathbf{n}, \quad \text{on } \Gamma_{m,v}, \tag{17}$$

where  $\boldsymbol{\epsilon} = \frac{1}{2} (\nabla \mathbf{u}_v + \nabla \mathbf{u}_v^T)$  is the rate of strain tensor given in the orthogonal coordinate system as

$$\epsilon_{\chi_1, \chi_1} = \frac{1}{h_1} \frac{\partial u_v}{\partial \chi_1} + \frac{v_v}{h_1 h_2} \frac{\partial h_1}{\partial \chi_2}, \tag{18}$$

$$\epsilon_{\chi_2, \chi_1} = \epsilon_{\chi_1, \chi_2} = \frac{h_2}{h_1} \frac{\partial}{\partial \chi_1} \left( \frac{v_v}{h_2} \right) + \frac{h_1}{h_2} \frac{\partial}{\partial \chi_2} \left( \frac{u_v}{h_1} \right). \tag{19}$$

*Slip Condition for Tangential Velocities on the Interface* This condition addresses the important issue of how the porous media affect the flow at the interface. [Beavers and Joseph \(1967\)](#) showed experimentally that a free fluid in contact with a porous medium flows faster than a fluid in contact with a solid surface. This observation is taken into account by imposing a slip boundary condition on the interface of the matrix and free fluid contact. Later, [Saffman \(1971\)](#) showed that this slip is independent from the tangential velocity in the porous domain.

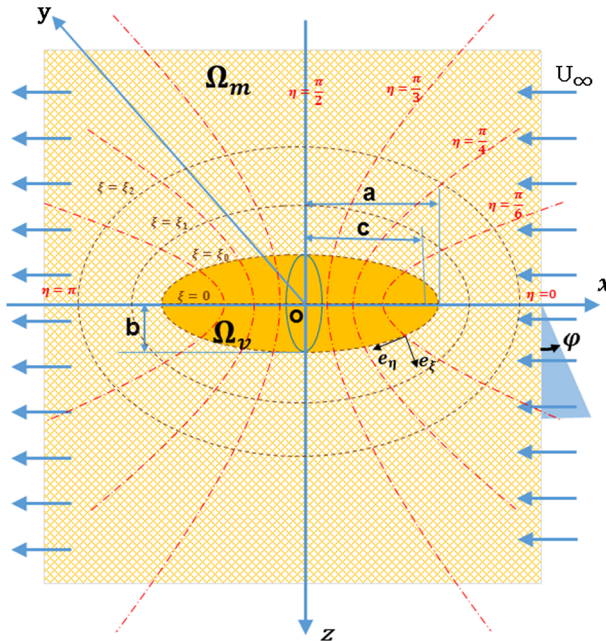


**Fig. 3** Spheroidal coordinates and a schematic of a spheroidal vug in the matrix

In the current work, we use the generalized form of Beavers–Joseph–Saffman slip boundary condition proposed by Jones (1973). Thus, for complicated interface geometries other than the plane interface, the generalized form of the slip boundary condition can be expressed as

$$\mathbf{n} \cdot \boldsymbol{\epsilon} \cdot \boldsymbol{\tau}_i = \frac{\lambda}{\sqrt{\boldsymbol{\tau}_i \cdot k_m \cdot \boldsymbol{\tau}_i}} \mathbf{u}_v \cdot \boldsymbol{\tau}_i, \quad i = 1, 2 \quad \text{on } \Gamma_{m,v}, \tag{20}$$

where  $\lambda$  is an empirical coefficient,  $k_m$  is the permeability of the matrix domain, and  $\boldsymbol{\tau}_i$  is the tangential unit vector to the interface (Fig. 2). Note that for axis-symmetric problems,  $i = 1$  in the slip boundary condition.

### 3 Spheroidal Vug

Stream function in the vug domain and pore pressure in the host homogeneous porous media can be analytically solved for certain geometries. Knowing these two functions, the other characteristics of flow can be determined in the ensemble of the domain. In this study, we present analytic solutions for vugs of prolate spheroidal shapes. The analytic solution for oblate spheroid can be easily obtained using the same methodology.

Let us consider one prolate spheroidal fluid-filled vuggy inclusion  $\Omega_v$  located in the homogeneous matrix medium  $\Omega_m$  with major axis  $a$  in the  $x$ -direction and minor axis  $b$  in the  $y, z$  directions with  $a > b$  as shown in Fig. 3.

We employ the prolate spheroidal coordinate system  $(\xi, \eta, \phi)$  with unit normal vectors  $(\mathbf{e}_\xi, \mathbf{e}_\eta, \mathbf{e}_\phi)$ , which is related to the Cartesian coordinate system through



$$\begin{aligned} x &= c \cosh \xi \cos \eta, \\ y &= c \sinh \xi \sin \eta \sin \phi, \\ z &= c \sinh \xi \sin \eta \cos \phi, \end{aligned} \tag{21}$$

with

$$0 \leq \xi < \infty, \quad 0 \leq \eta \leq \pi, \quad 0 \leq \phi \leq 2\pi, \tag{22}$$

and the focal length of the spheroid  $c$  as

$$c = \sqrt{a^2 - b^2}, \tag{23}$$

For the sake of the notational convenience, the following change of variables is introduced

$$s = \cosh \xi, \quad t = \cos \eta, \tag{24}$$

and then,

$$\begin{aligned} x &= cst, \\ y &= c\sqrt{s^2 - 1}\sqrt{1 - t^2} \sin \phi, \\ z &= c\sqrt{s^2 - 1}\sqrt{1 - t^2} \cos \phi. \end{aligned} \tag{25}$$

The coordinates of any point inside of the spheroidal vug is given by

$$\Omega_v = \{(s, t, \phi) : 1 \leq s \leq s_o, \quad -1 \leq t \leq 1, \quad 0 \leq \phi \leq 2\pi\}, \tag{26}$$

with  $s_o = a/c$ , which defines the prolate spheroid of semi-axes  $a, b$ . One can see that use of the spheroidal coordinate system facilitates the definition of the boundary condition on the contact of vug and porous media in terms of the boundary condition on  $s = s_o$ . Besides, the  $E^2$  and  $\nabla^2$  operators remain separable with respect to the spheroidal coordinate system variables.

The prolate spheroidal coordinate scale factors are as follows

$$h_1 = h_2 = c\sqrt{s^2 - t^2}, \quad h_3 = c\sqrt{s^2 - 1}\sqrt{1 - t^2}. \tag{27}$$

Using  $(s, t, \phi)$  as the new coordinate variables leads to the following differential equation

$$\frac{\partial}{\partial \xi} = \sqrt{s^2 - 1} \frac{\partial}{\partial s}, \quad \frac{\partial}{\partial \eta} = -\sqrt{1 - t^2} \frac{\partial}{\partial t}. \tag{28}$$

### 3.1 Fluid Flow Inside the Spheroidal Vug

We apply the same method introduced by [Dassios et al. \(1994\)](#) to solve the axis-symmetric Stokes flow in the spheroidal coordinate system. Inside the spheroidal vug, the Stokes stream function should satisfy Eq. 10, where the differential operator  $E^2$  in the spheroidal coordinate system is given as

$$E^2 = \frac{1}{c^2(s^2 - t^2)} \left[ (s^2 - 1) \frac{\partial^2}{\partial s^2} + (1 - t^2) \frac{\partial^2}{\partial t^2} \right]. \tag{29}$$

We define the kernel of  $E^2$  denoted by  $\text{Ker}E^2$  as ensemble of all functions  $f$  that  $f$  satisfies  $E^2 f = 0$ . Similarly, if a function  $f$  satisfies  $E^4 f = 0$ , it belongs to the kernel of  $E^4$  denoted by  $\text{Ker}E^4$ . We introduce the following series expansion for the stream function  $\Psi_v$

decomposed into two parts, the part already in  $\text{Ker}E^2$  and the part not in  $\text{Ker}E^2$ , but still in  $\text{Ker}E^4$ ; thus, resulting in

$$\Psi_v(s, t) = c^2\Phi(s, t) + c^2\Theta(s, t), \quad \text{in } \Omega_v. \tag{30}$$

$\Theta(s, t)$  belongs to the  $\text{Ker}E^2$  which gives

$$E^2\Theta = 0. \tag{31}$$

$\Theta(s, t)$  is a trivial solution for  $\text{Ker}E^4$ .  $\Phi(s, t)$  represents the remainder of the functions in  $\text{Ker}E^4$  which do not belong to  $\text{Ker}E^2$

$$E^2\Phi \neq 0, \quad E^4\Phi = 0. \tag{32}$$

The coefficient  $c^2$  preceding either of the terms on the right-hand side of Eq. 30 is for additional formulation convenience. In the following subsections, we define  $\Theta$  and  $\Phi$  separately.

*Functions in  $\text{Ker}E^2$*

Using the technique of separation of variables, it becomes possible to verify that  $\Theta(s, t) \in \text{Ker}E^2$  can be expressed in the form of a series as

$$\Theta(s, t) = \sum_{i=1}^4 \sum_{n=0}^{\infty} a_{i,n} \Theta_{i,n}(s, t), \tag{33}$$

where  $a_{i,n}$  are the constants to be defined and  $\Theta_{i,n}$  is given by

$$\Theta_{1,n}(s) = G_n(s)G_n(t), \tag{34a}$$

$$\Theta_{2,n}(s) = G_n(s)H_n(t), \tag{34b}$$

$$\Theta_{3,n}(s) = H_n(s)G_n(t), \tag{34c}$$

$$\Theta_{4,n}(s) = H_n(s)H_n(t), \tag{34d}$$

where  $G_n$  and  $H_n$  are the Gegenbauer polynomials of first and second kind and of degree  $-\frac{1}{2}$ , which is given in ‘‘Appendix 1.’’

*Functions in  $\text{Ker}E^4$*

We look for the functions  $\Phi(s, t)$  with  $E^2\Phi \in \text{Ker}E^2$ , and then  $\Phi \in \text{Ker}E^4$ . Let us introduce the following series expansion for  $\Phi(s, t)$  as

$$\Phi(s, t) = \sum_{i=1}^4 \sum_{n=0}^{\infty} \Phi_{i,n}(s, t). \tag{35}$$

Then, the stream function inside the vug will be rewritten as

$$\Psi_v(s, t) = \sum_{i=1}^4 (\Psi_v)_i(s, t) = c^2 \sum_{i=1}^4 \sum_{n=0}^{\infty} \Phi_{i,n}(s, t) + c^2 \sum_{i=1}^4 \sum_{n=0}^{\infty} \Theta_{i,n}(s, t). \tag{36}$$

The functions  $\Phi_{i,n}(s, t)$  are defined so that

$$E^2\Phi_{i,n}(s, t) = C_{i,n}\Theta_{i,n}(s, t), \quad \text{in } \Omega_v, \tag{37}$$

for  $i = 1, \dots, 4, \quad n = 0, 1, 2, \dots$ , where  $C_{i,n}$  is the constant to be defined later. One can deduce from the previous equations that

$$E^4\Phi_{i,n}(s, t) = E^2(E^2\Phi_{i,n}(s, t)) = C_{i,n}E^2\Theta_{i,n}(s, t) = 0. \tag{38}$$

Let us study Eq. 37 for  $i = 1$

$$\left[ (s^2 - 1) \frac{\partial^2}{\partial s^2} + (1 - t^2) \frac{\partial^2}{\partial t^2} \right] \Phi_{1,n}(s, t) = c^2 C_{1,n}(s^2 - t^2) G_n(s) G_n(t). \tag{39}$$

In general, the equation in the form of

$$\left[ (s^2 - 1) \frac{\partial^2}{\partial s^2} + (1 - t^2) \frac{\partial^2}{\partial t^2} \right] U(s, t) = f_m(s) g_n(t), \tag{40}$$

where  $f_m$  and  $g_n$  are the Gegenbauer polynomials of the first or second kind and of order  $n$  and  $m$ , with  $n \neq m$  and  $n + m \neq 1$ , has a particular solution defined in terms of a separable function as

$$U_{n,m}(s, t) = \frac{f_m(s) g_n(t)}{(n - m)(n + m - 1)}. \tag{41}$$

Using relations given by Eqs. 85 and 86 in ‘‘Appendix 1,’’ the terms including  $s^2$  and  $t^2$  on the right-hand side (RHS) of Eq. 39 are absorbed into Gegenbauer polynomials. Consequently, the solution of Eq. 39 is

$$\begin{aligned} \Phi_{1,n}(s, t) = c^2 C_{1,n} & \left( \frac{-\alpha_n}{2(2n - 1)} G_{n-2}(s) + \frac{\beta_n}{2(2n + 1)} G_{n+2}(s) \right) G_n(t) \\ & - c^2 C_{1,n} G_n(s) \left( \frac{\alpha_n}{2(2n - 1)} G_{n-2}(t) - \frac{\beta_n}{2(2n + 1)} G_{n+2}(t) \right), \end{aligned} \tag{42}$$

where  $\alpha_n, \beta_n, \gamma_n$  for  $n \geq 4$  are given by Eq. 87 in ‘‘Appendix 1.’’ As long as we just use the terms including Gegenbauer polynomials of first kind, one can redefine  $\alpha_n, \beta_n, \gamma_n$  for  $n < 4$ , as

$$\begin{aligned} \alpha_0 = \alpha_1 = \alpha_2 = \alpha_3 & = 0, \\ \gamma_0 = 1, \quad \gamma_1 = 1, \quad \gamma_2 & = \frac{1}{5}, \quad \gamma_3 = \frac{3}{7}, \\ \beta_0 = -2, \quad \beta_1 = 2, \quad \beta_2 & = \frac{4}{5}, \quad \beta_3 = \frac{4}{7}. \end{aligned} \tag{43}$$

Note that  $\Phi_{1,n}$  only includes the particular solution to nonhomogeneous Eq. 37 and the solution to the homogeneous problem will be included in  $\Theta_{1,n}$ . Therefore,  $(\Psi_v)_1$  includes the complete set of the solution as follows

$$(\Psi_v)_1(s, t) = c^2 \sum_{n=0}^{\infty} \Phi_{1,n}(s, t) + c^2 \sum_{n=0}^{\infty} a_{1,n} \Theta_{1,n}(s, t), \tag{44}$$

which can be written as

$$(\Psi_v)_1(s, t) = c^2 \sum_{n=1}^{\infty} g_{1,n}(s) G_n(t), \tag{45}$$

with

$$\begin{aligned} g_{1,n} = a_{1,n} G_n(s) + c^2 & \left( \frac{\beta_{n-2} C_{1,n-2}}{2(2n - 3)} - \frac{\alpha_n C_{1,n}}{2(2n - 1)} \right) G_{n-2}(s) \\ & + c^2 \left( \frac{\beta_n C_{1,n}}{2(2n + 1)} - \frac{\alpha_{n+2} C_{1,n+2}}{2(2n + 3)} \right) G_{n+2}(s). \end{aligned} \tag{46}$$

Applying the same procedure for  $\Phi_{2,n}(s, t), \Phi_{3,n}(s, t), \Phi_{4,n}(s, t)$  in Eq. 37, and associating the terms including Gegenbauer polynomials of  $t$  of the same order, the complete set

of solutions for Stokes stream function can be determined. In our work, the general solution for Stokes stream function can be simplified using the following assumptions:

- The solution has to be bounded on the axis of symmetry; thus,  $i$  is limited to  $i = 1, 3$  in Eq. 36 regarding to the definition of  $\Theta_{i,n}$  given in Eq. 34.
- The solution has symmetry with respect to  $t$  and then only the even  $n$  values are used,  $n = 2k$ .
- The solution has to be bounded inside the spheroidal vug when  $s \rightarrow 1$  and then  $i$  is limited to  $i = 1$ , regarding to the definition of  $\Theta_{i,n}$  given in Eq. 34.

Eventually, the stream function inside the spheroidal vug is given as

$$\psi_v(s, t) = c^2 \sum_{k=1}^{\infty} g_{1,2k}(s)G_{2k}(t). \tag{47}$$

Note that none of the individual terms in Eq. 47 satisfies  $E^4\psi_v(s, t) = 0$ , but the sum of all the other terms do. This condition can be investigated using the method for developing the solution.

Once the stream function in the vug is defined, we can determine the pressure field inside the vug using Eqs. 12 and 28 as follows

$$\begin{aligned} (s^2 - 1) \frac{\partial p_v}{\partial s} &= -\frac{\mu}{c\rho} \frac{\partial}{\partial t} (E^2\psi_v), \\ (1 - t^2) \frac{\partial p_v}{\partial t} &= \frac{\mu}{c\rho} \frac{\partial}{\partial s} (E^2\psi_v), \end{aligned} \tag{48}$$

and the pressure field inside the spheroidal vug is given as

$$p_v(s, t) = - \sum_{k=1}^{\infty} \frac{\mu c}{2k(2k - 1)} C_{1,2k} P_{2k-1}(s)P_{2k-1}(t). \tag{49}$$

$P_n(t)$  is the Legendre polynomial of first kind and order  $n$ .

### 3.2 Fluid Flow in the Matrix Domain Outside the Spheroidal Vug

The host porous media pressure field outside the vug should satisfy the Laplacian equation given by Eq. 3, with the Laplacian differential operator given for the spheroidal coordinate system as

$$\nabla^2 = \frac{1}{c^2(s^2 - t^2)} \left[ (s^2 - 1) \frac{\partial^2}{\partial s^2} + (1 - t^2) \frac{\partial^2}{\partial t^2} + 2s \frac{\partial}{\partial s} - 2t \frac{\partial}{\partial t} \right]. \tag{50}$$

Considering the regularity of the far field pressure in Eq. 15 as

$$\lim_{s \rightarrow \infty} p_m(s, t) = |\nabla(p_m)_\infty| c s t, \tag{51}$$

the pressure field outside the spheroidal vug is given by

$$p_m(s, t) = \sum_{k=1}^{\infty} c F_{2k-1}(s) P_{2k-1}(t), \tag{52}$$

with

$$F_{2k-1}(s) = |\nabla(p_m)_\infty| s \delta_{1,2k-1} + A_{2k} Q_{2k-1}(s), \tag{53}$$

where  $\delta_{1,2k-1}$  is the Kronecker delta function,  $Q_n(s)$  is the Legendre polynomial of second kind and order  $n$ , and  $A_{2k}$  are the coefficients to be determined later. As the pressure field has to be odd with respect to the axis of symmetry, only odd terms are included in this solution. Note that

$$\lim_{s \rightarrow \infty} \frac{Q_{2k-1}(s)P_{2k-1}(t)}{cst} = 0. \tag{54}$$

The stream function in Darcy’s domain is obtained through the definition of the velocity field using Eq. 6 as

$$\begin{aligned} (s^2 - 1) \frac{\partial p_m}{\partial s} &= -\frac{\mu}{k_m c \rho} \frac{\partial \Psi_m}{\partial t}, \\ (1 - t^2) \frac{\partial p_m}{\partial t} &= \frac{\mu}{k_m c \rho} \frac{\partial \Psi_m}{\partial s}. \end{aligned} \tag{55}$$

The stream function outside the spheroidal vug is given by

$$\Psi_m(s, t) = -\frac{c^2 k_m (s^2 - 1)(1 - t^2)}{\mu 2k(2k - 1)} F'_{2k-1}(s) P'_{2k-1}(t), \tag{56}$$

where ' denotes derivative. It can be shown that

$$\lim_{x \rightarrow \infty} \Psi_m = \frac{1}{2} U_\infty r^2, \tag{57}$$

where  $r^2 = c^2(s^2 - 1)(1 - t^2)$  and  $U_\infty = -\frac{k_m}{\mu} |\nabla(p_m)_\infty|$ .

### 3.3 Coupling Matrix and Stokes Domains

The undetermined coefficients of the stream function in the vug and the pressure field in host porous media can be determined by imposing the boundary conditions given in Eqs. 16, 17 and 20. The condition given by Eq. 16 in the spheroidal coordinates is as follows

$$\frac{\partial \Psi_v}{\partial t} = \frac{\partial \Psi_m}{\partial t}, \quad \text{on } s = s_o, \tag{58}$$

which after associating the coefficients of the same  $t$ -dependent functions yields

$$g_{1,2k}(s_o) = -\frac{k_m}{2k(2k - 1)\mu} (s_o^2 - 1) F'_{2k}(s_o). \tag{59}$$

The generalized Beavers–Joseph–Saffman condition described in Eq. 20, with the tangential component of the rate of the strain tensor  $\epsilon_{\xi\eta} = \epsilon_{\eta\xi}$  given as

$$\begin{aligned} \epsilon_{\xi\eta} = \frac{1}{c^3} \left[ \sqrt{\frac{(s^2 - 1)}{(1 - t^2)}} \left( \frac{-2s}{(s^2 - t^2)^2} \frac{\partial \Psi_v}{\partial s} + \frac{1}{(s^2 - t^2)} \frac{\partial^2 \Psi_v}{\partial s^2} \right) \right. \\ \left. - \sqrt{\frac{(1 - t^2)}{(s^2 - 1)}} \left( \frac{2t}{(s^2 - t^2)^2} \frac{\partial \Psi_v}{\partial t} + \frac{1}{(s^2 - t^2)} \frac{\partial^2 \Psi_v}{\partial t^2} \right) \right], \end{aligned}$$

reduces to

$$\begin{aligned} \left( -2s \frac{\partial \Psi_v}{\partial s} + (s^2 - t^2) \frac{\partial^2 \Psi_v}{\partial s^2} \right) - \left( 2t \frac{\partial \Psi_v}{\partial t} + (s^2 - t^2) \frac{\partial^2 \Psi_v}{\partial t^2} \right) \\ = \frac{c\lambda}{\sqrt{k_m}} \sqrt{s^2 - 1} (s^2 - t^2)^{\frac{3}{2}} \frac{\partial \Psi_v}{\partial s}, \quad \text{on } s = s_o. \end{aligned} \tag{60}$$

Replacing the Stokes stream function from Eq. 47 yields the following equation

$$\begin{aligned} & \sum_{k=1}^{\infty} -\frac{2s_o(s_o^2 - 1)}{2k(2k - 1)} g'_{1,2k}(s_o) P'_{2k-1}(t) \\ & + \left[ \frac{s_o^2 - 1}{2k(2k - 1)} g''_{1,2k}(s_o) + g_{1,2k}(s_o) \right] (s_o^2 - t^2) P'_{2k-1}(t) \\ & + 2g_{1,2k}(s_o)t P_{2k-1}(t) = \sum_{k=1}^{\infty} \frac{\lambda c}{\sqrt{k_m}} \frac{\sqrt{s_o^2 - 1}}{2k(2k - 1)} g'_{1,2k}(s_o) (s_o^2 - t^2)^{\frac{3}{2}} P'_{2k-1}(t). \end{aligned} \tag{61}$$

It is complicated to separate the coefficients of  $P_{2k-1}(t)$  or  $P'_{2k-1}(t)$  for Eq. 61 in order to equalize the coefficients of the same terms. We rewrite all the terms in the form of Legendre polynomial expansion series. For computational purposes, this is a good technique for working with nonsimilar terms. Using the Legendre series expansion as shown in “Appendix 2,” all of the terms in Eq. 61 are expressed in terms of  $P_{2n}(t)$ , and we can equalize the similar terms.

The pressure jump condition given by Eq. 17 in the spheroidal coordinate system with

$$\epsilon_{\xi\xi} = \frac{1}{c^3(s^2 - t^2)} \left( \frac{\partial^2 \Psi_v}{\partial s \partial t} + \frac{t}{s^2 - t^2} \frac{\partial \Psi_v}{\partial s} - \frac{s(2s^2 - 1 - t^2)}{(s^2 - t^2)(s^2 - 1)} \frac{\partial \Psi_v}{\partial t} \right), \tag{62}$$

and is given as

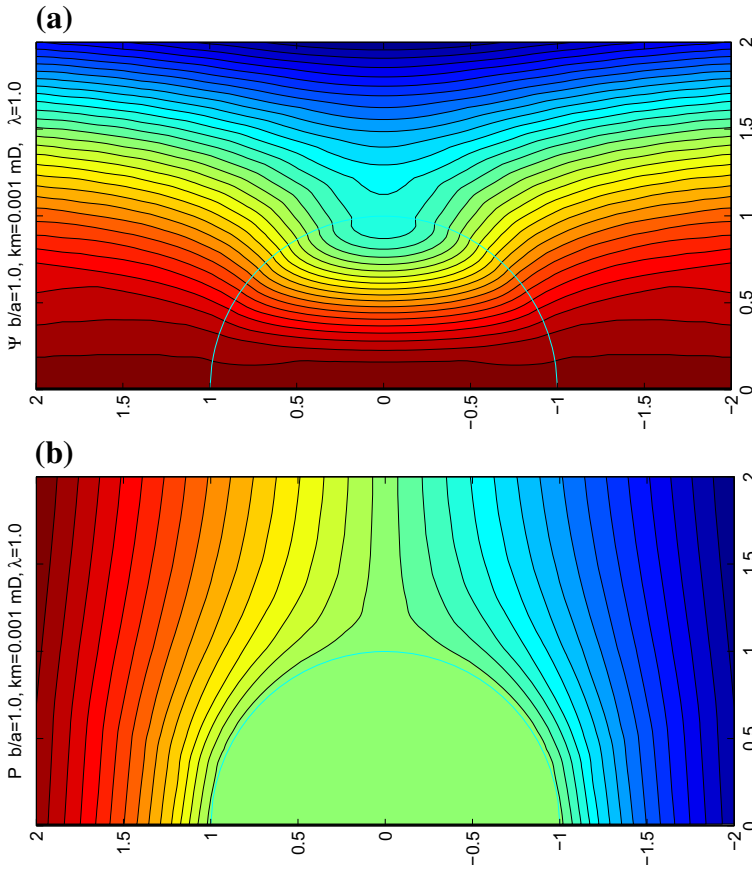
$$\begin{aligned} & \sum_{k=1}^{\infty} \frac{c^2}{2} \left( C_{1,2k} P_{2k-1}(s_o) + F_{2k-1}(s)/\mu \right) (s_o^2 - t^2)^2 P_{2k-1}(t) \\ & = \sum_{k=1}^{\infty} g'_{1,2k}(s_o) (s_o^2 - t^2) P_{2k-1}(t) \\ & - \sum_{k=1}^{\infty} g'_{1,2k}(s_o)t G_{2k}(t) - \sum_{k=1}^{\infty} g_{1,2k}(s_o) \frac{s_o(2s_o^2 - 1 - t^2)}{s_o^2 - 1} P_{2k-1}(t). \end{aligned} \tag{63}$$

We rewrite all of the terms in the form of the Legendre polynomial series expansion and equalize the similar terms. For the sake of computational ease, we replace the infinite sum  $\sum_{k=1}^{\infty}$  with finite sum  $\sum_{k=1}^N$  with  $N \geq 1$ . Having  $3N$  equations given by Eqs. 59, 61, and 63, we can obtain  $3N$  unknowns  $C_{1,2k}$ ,  $a_{1,2k}$ ,  $A_{2k}$  by solving an algebraic linear system of equations.

In “Appendix 5,” it is shown that when the spheroidal semi-focal distance tends to zero the flow problem reduces to problem of flow in porous domain with spherical vugs which is expected to be so.

Figure 4 shows the pressure field and streamlines in a matrix cell, including a spheroidal vug with aspect ratio equal to 1. The streamlines in the area near the vug tend to pass through the fluid-filled vug, which has less resistance through which to pass. The pressure remains constant inside the vug, which means negligible pressure drop occurs in the vug.

The effect of the Beavers–Joseph–Saffman coefficient on the flow is shown in Fig. 5. As  $\frac{\sqrt{k_m}}{\lambda}$  becomes larger, the streamlines are no longer continuous on the interface of the matrix and vug domains, and the tangential component of the velocity in the vug domain becomes much more significant. Because the tangential component of the velocity on the interface on the matrix side is negligible, the inflow and outflow to and from the matrix domain is normal to the interface.



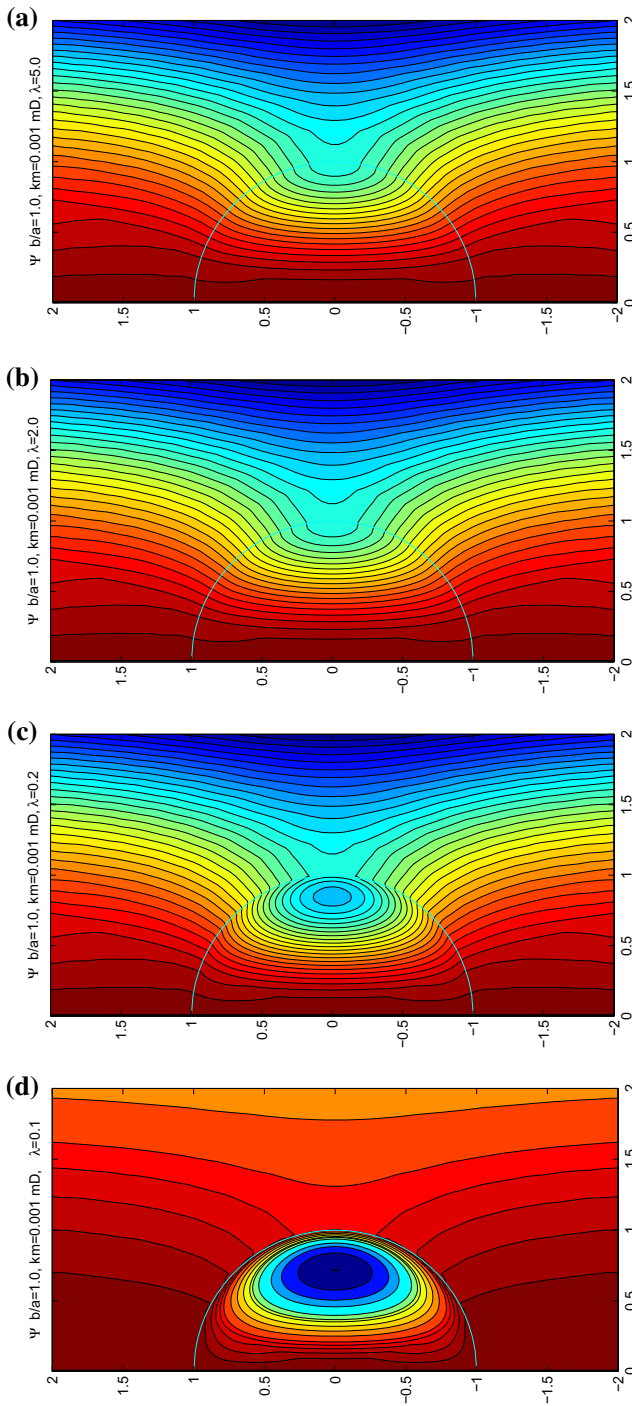
**Fig. 4** Streamline and pressure field in a porous medium, including vuggy inclusion  $b/a = 1$ . **a** Streamline. **b** Pressure field

Figure 6 shows the flow field for different aspect ratios of the vuggy inclusion. As shown, the fluid in the matrix domain tends to pass through the vug. Inside the vug, the streamline tends to be a straight line in the general direction of the flow close to the longitudinal axis of the vug.

Figure 7 shows an example of fluid flow in a matrix cell, including randomly distributed vugs with various aspect ratios. The objective here is to develop a method for determining the effective permeability of such a domain. In the next section, we will determine the equivalent permeability of a single spheroidal vug.

### 4 Equivalent Permeability of a Single Spheroidal Vug

The equivalent permeability of a fluid-filled prolate spheroidal vug  $\Omega_v$  in a porous matrix  $\Omega_m$  will be determined in this section. We assume that the spheroidal vug can be replaced by a porous inclusion that creates the same flow field exterior to the vug. We determine the flow properties of this porous inclusion notably its permeability which can be considered as the



**Fig. 5** Streamlines in the matrix medium with a permeability of  $k_m = 0.001$  mD through a spheroidal vug of  $b/a = 1$  for several Beavers–Joseph coefficients. **a**  $\lambda = 5$ . **b**  $\lambda = 2$ . **c**  $\lambda = 0.2$ . **d**  $\lambda = 0.1$



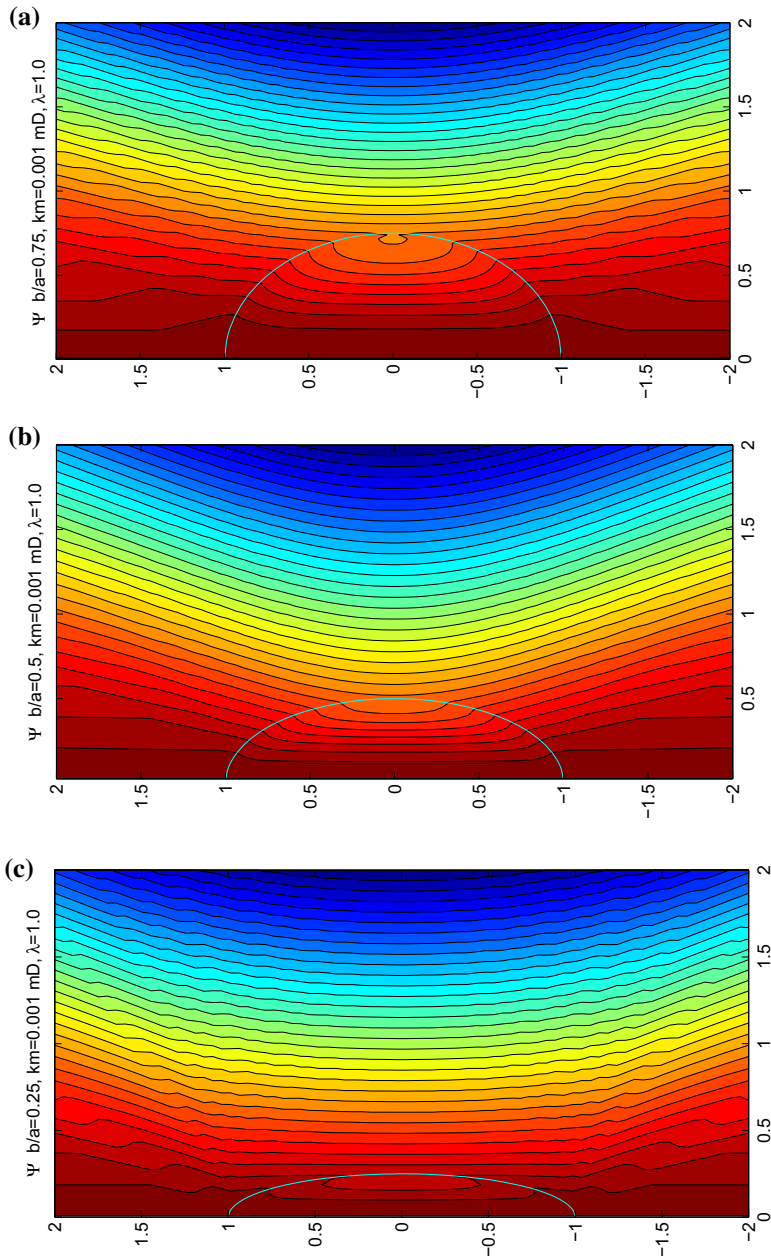


**Fig. 6** Fluid flow in the matrix medium with a permeability of  $k_m = 0.001$  mD through spheroidal vugs with various aspect ratios. The local corrugations are due to very close numerical precision of stream function values. **a**  $b/a = 0.75$ . **b**  $b/a = 0.5$ . **c**  $b/a = 0.25$

equivalent permeability of the vug. The permeability of a porous inclusion  $(\Omega_m)_{in}$  of same size as the fluid-filled vug which generates the same pressure field in the matrix domain will be obtained. The pressure inside the porous spheroidal inclusion should satisfy the Laplacian

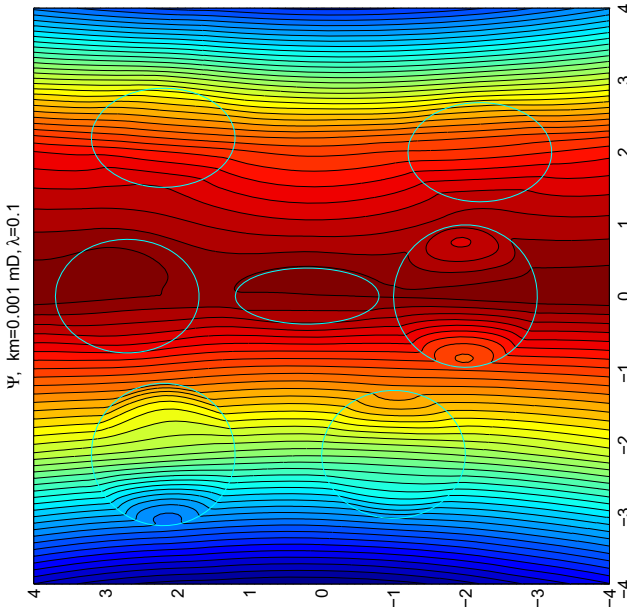


**Fig. 7** Streamlines for a matrix domain with a permeability of  $k_m = 0.001$  mD with spheroidal vugs scattered through with the Beavers–Joseph coefficient  $\lambda = 0.1$

equation. We apply the method of separation of variables to the Laplacian equation. In fact, we assume that the solution to the Laplacian equation in the spheroidal coordinate system can be found in terms of multiplication of two sets of pure functions of  $s, t$  the independent variables of the spheroidal coordinate system. Considering the condition of bounded pressure at the center of inclusion, the pressure inside the porous spheroidal inclusion is given as

$$(p_m)_{in} = c \sum_{k=1}^{\infty} D_{2k} P_{2k-1}(s) P_{2k-1}(t), \quad \text{in } (\Omega_m)_{in} \tag{64}$$

where  $(p_m)_{in}$  represents the pressure in the porous spheroidal inclusion. This means that the first approximation of the stream function inside the porous inclusion is a straight line, which is a result of using Darcy’s law for describing the fluid flow inside the inclusion.

The boundary condition for coupling a porous inclusion and the matrix medium is the no-jump boundary condition for the pressures and the normal fluxes on the interface given as

$$p_m = (p_m)_{in}, \quad \text{on } s = s_o, \tag{65}$$

$$\frac{k_m}{\mu} \frac{\partial p_m}{\partial s} = \frac{(k_m)_{in}}{\mu} \frac{\partial (p_m)_{in}}{\partial s}, \quad \text{on } s = s_o, \tag{66}$$

where  $p_m$  is given in Eq. 52, and  $(k_m)_{in}$  is the permeability of the porous inclusion which is the equivalent permeability of the spheroidal vug that is determined. After associating the coefficient of terms  $P_{2k-1}(t)$ , we determine the undetermined coefficients of pressure in the porous inclusion as

$$D_{2k} = \frac{F_{2k-1}(s_o)}{P_{2k-1}(s_o)}. \tag{67}$$

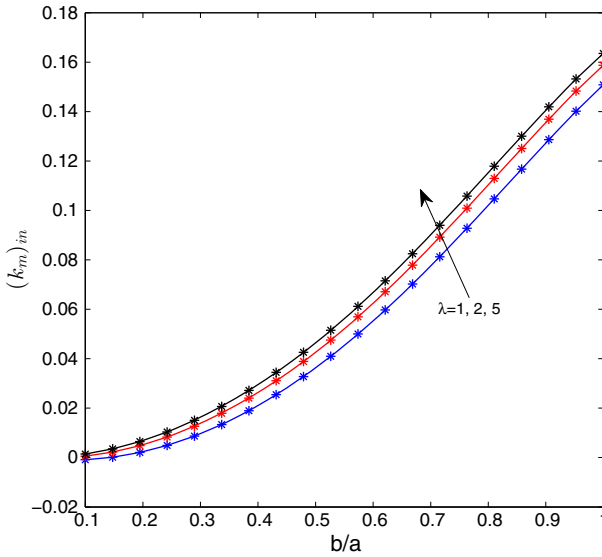


**Fig. 8** Effect of aspect ratio and the Beavers–Joseph–Saffman coefficient on the equivalent permeability of a spheroidal vug for  $k_m = 0.001mD$

Finally, the equivalent permeability of a prolate spheroidal vug with outer spheroid  $s_o$  located in a homogeneous matrix of permeability  $k_m$  is given as

$$(k_m)_{in} = k_m \frac{\sum_{k=1}^{\infty} F'_{2k-1}(s_o)}{\sum_{k=1}^{\infty} \frac{F_{2k-1}(s_o)}{P_{2k-1}(s_o)} P'_{2k-1}(s_o)}. \tag{68}$$

Note that this is the component of the permeability tensor in the direction of the larger semi-axis of prolate spheroid.

In Fig. 8, the equivalent permeability for a spheroidal vug is plotted for various aspect ratios. The highest permeability is for the spherical vug when the aspect ratio  $b/a$  is equal to 1. For a fix value of  $a$ , as the vug becomes more elongated, its volume fraction reduces and, respectively, the equivalent permeability reduces. For low aspect ratios, i.e., in the case of this figure for  $b/a < 0.1$  the medium can be assumed as a homogeneous medium. In other words, nonconnected narrow fractures can be ignored.

The effect of Beavers–Joseph–Saffman boundary condition on the equivalent permeability of the spheroidal vug is shown in Fig.8. For larger values of the Beavers–Joseph–Saffman coefficient  $\lambda$ , as the streamlines on the interface are semi-continuous, the equivalent permeability of the vug is higher than the case of lower values of  $\lambda$ , where a rotation zone appears inside the vug due to the inclination of the streamlines.

Figure 9 shows that the equivalent permeability of a spheroidal vug located in a higher permeable matrix is less than the equivalent permeability of the same vug placed in a lower permeable matrix. The higher permeable host media reduces the effect of presence of vugs.

Figure 9, illustrates the role of the host matrix permeability on the equivalent permeability of a spheroidal vug. The equivalent permeability of a spheroidal vug placed in a high permeable matrix is less than the equivalent permeability of the same vug placed in a low

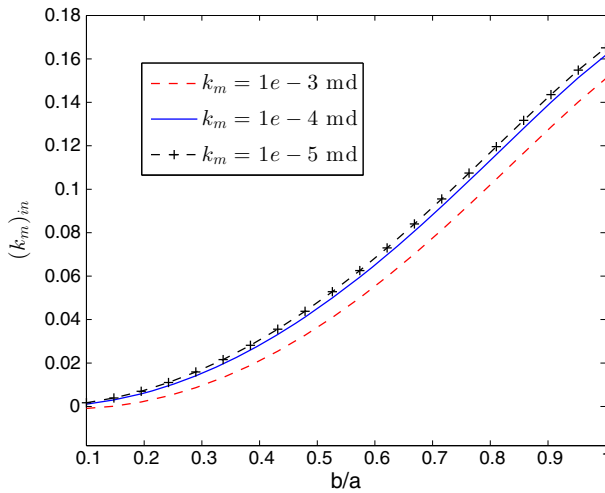


**Fig. 9** Effect of the matrix permeability on the equivalent permeability of a spheroidal vug for  $\lambda = 1$

permeable host matrix. The more permeable the host matrix is the role of the vug is less significant.

## 5 Effective Permeability of the Matrix Medium Including Spheroidal Vugs

Previously, we substituted the fluid-filled vug with its equivalent porous inclusion having an equivalent permeability, but greater than the permeability of the host matrix. Now, the matrix domain under consideration consists of a set of locally homogeneous porous regions. The effective permeability of the entire nonhomogeneous porous domain is desired.

The effective medium theory provides the effective permeability for a binary medium, where all the inhomogeneities are identical in shape, orientation, size, and physical properties. The effective medium theory is based on analyzing the perturbation of one single inhomogeneity located at the center of porous matrix and superposition of the remaining inhomogeneities effect, assuming they can be considered to be at the center and have no interference with other inhomogeneities.

Three formulas widely used in the field of effective medium theory are the Maxwell formula, the self-consistent (or symmetric Bruggeman) formula and the differential or asymmetric (Bruggeman 1935) formula. The Maxwell formula is widely used of the three equations. The Maxwell formula for the effective permeability of a binary domain including porous spheroidal inclusions is given as

$$(k)_{\text{eff}} = k_m + \frac{\omega((k_m)_{\text{in}} - k_m)}{1 + d_i(1 - \omega)((k_m)_{\text{in}} - k_m)/k_m}, \quad (69)$$

where  $k_{\text{eff}}$  is the effective permeability of the entire porous medium,  $\omega$  is the volume fraction of inclusions,  $k_m$  is the permeability of the host matrix,  $(k_m)_{\text{in}}$  is the equivalent permeability of one inclusion, and  $d_i$  is the depolarization coefficient for a given direction. In general, the Maxwell formula provides reasonable results for isotropic assemblages of nonoverlapping inclusions in binary media.

Another method for determining the effective permeability of a nonhomogeneous porous medium is by upscaling through the direct solution of the steady-state problem. In this method, the equivalent permeability tensor for an arbitrary nonhomogeneous upscaling cell is calculated from the solution of the steady-state flow equation in a domain that corresponds to the upscaling cell itself. The equivalent permeability tensor is computed in such a way that Darcy’s law between the volume averages of the small-scale fluxes and field-scale volumetric fluxes and gradients is satisfied (Rubin and Gómez-Hernández 1990), i.e.,

$$-k_{\text{eff}} = \frac{-\langle k \nabla p \rangle}{\langle \nabla p \rangle}, \tag{70}$$

where  $k$  is the local permeability, and the angular brackets imply the volume integral defined as

$$\langle f \rangle = \int_V f \, dv. \tag{71}$$

Let us determine the effective permeability of a spherical porous cell of radius  $\rho_1$ , including one spherical fluid-filled vug of radius  $\rho_o < \rho_1$  located at the center of a matrix volume. The pressure field  $(p_m)_{\text{in},s}$  inside the vug’s equivalent spherical porous inclusion and the pressure field  $(p_m)_s$  outside the spherical vug in the matrix are given in “Appendix 4” in Eqs. 105, 115 as

$$\begin{aligned} (p_m)_{\text{in},s} &= D_{\text{in}} \rho \cos \theta, \quad 0 \leq \rho \leq \rho_o, \\ (p_m)_s &= \left( \frac{D}{\rho^2} + |\nabla(p_m)_\infty| \right) \cos \theta, \quad \rho_o \leq \rho \leq \rho_1, \end{aligned} \tag{72}$$

where  $D, D_{\text{in}}$  are coefficients to be determined later. The volume average of the pressure field in the entire domain is expressed as the sum of volume average of pressure in the porous inclusion and in the matrix written as

$$\left\langle \frac{\partial p}{\partial x} \right\rangle = \left\langle \frac{\partial (p_m)_{\text{in},s}}{\partial x} \right\rangle_{\text{in}} + \left\langle \frac{\partial (p_m)_s}{\partial x} \right\rangle_m. \tag{73}$$

In the spherical coordinates, the volume integral is given by

$$\langle f \rangle = \int_0^{2\pi} \int_0^\pi \int_0^{\rho_o} f(\rho, \theta, \phi) \rho^2 \sin \theta \, d\rho \, d\theta \, d\phi. \tag{74}$$

Because  $x = \rho \cos \theta$ , the pressure gradient in the  $x$  direction is given as

$$\begin{aligned} \frac{\partial (p_m)_{\text{in},s}}{\partial x} &= D_{\text{in}}, \\ \frac{\partial (p_m)_s}{\partial x} &= \frac{\partial (p_m)_s}{\partial \rho} \frac{1}{\cos \theta} - \frac{\partial (p_m)_s}{\partial \theta} \frac{1}{\rho^2 \sin \theta} = -\frac{D}{\rho^3} + |\nabla(p_m)_\infty|. \end{aligned} \tag{75}$$

Substituting this equation in Eq. 70 and performing the volume average of the steady-state solution yield the effective permeability of the porous volume, including one spherical vug in the center given by

$$k_{\text{eff}} = k_m + \frac{\omega((k_m)_{\text{in},s} - k_m)}{-\frac{\omega((k_m)_{\text{in},s} - k_m)}{k_m} \ln \frac{\rho_o}{\rho_1} + 1 + \frac{1}{3} \frac{(k_m)_{\text{in},s} - k_m}{k_m} (1 - \omega)}, \tag{76}$$

with  $(k_m)_{\text{in},s}$  given in Eq. 118. This equation is equivalent to Maxwell’s formula given in Eq. 69 if  $\frac{\rho_o}{\rho_1} \sim 1$ . As one can see, using Maxwell’s formula would result in **overestimating** the effective permeability.

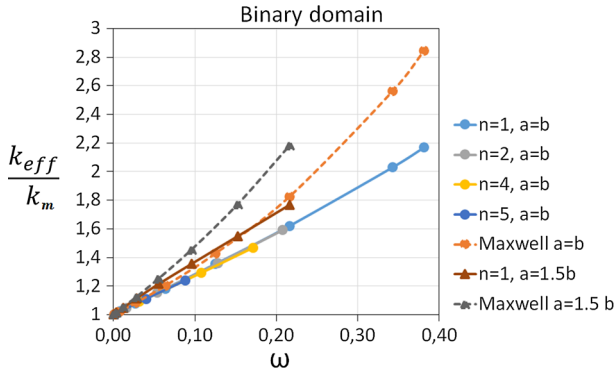


**Fig. 10** Normalized effective permeability of the porous domain, including spheroidal vugs versus  $\omega$  as vug volume fractions and  $n$  as number of vugs

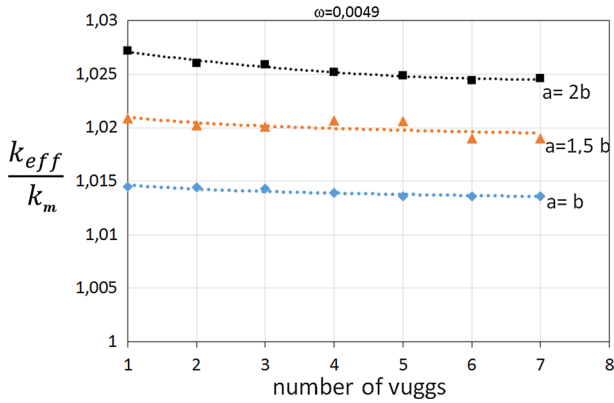


**Fig. 11** Effective permeability of a vuggy porous domain for a fixed-volume fraction of vugs  $\omega = 0.0049$  and various aspect ratios versus number of vugs with  $\lambda = 1, k_m = 0.001$  mD

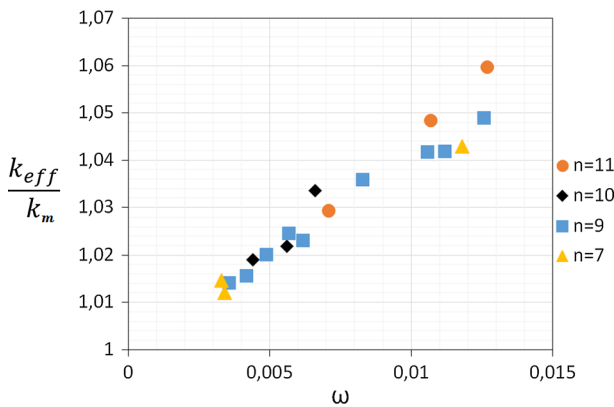


**Fig. 12** Effective permeability of a vuggy porous domain with several spheroidal vugs randomly distributed in domain and with random aspect ratios for  $\lambda = 1, k_m = 0.001$  mD

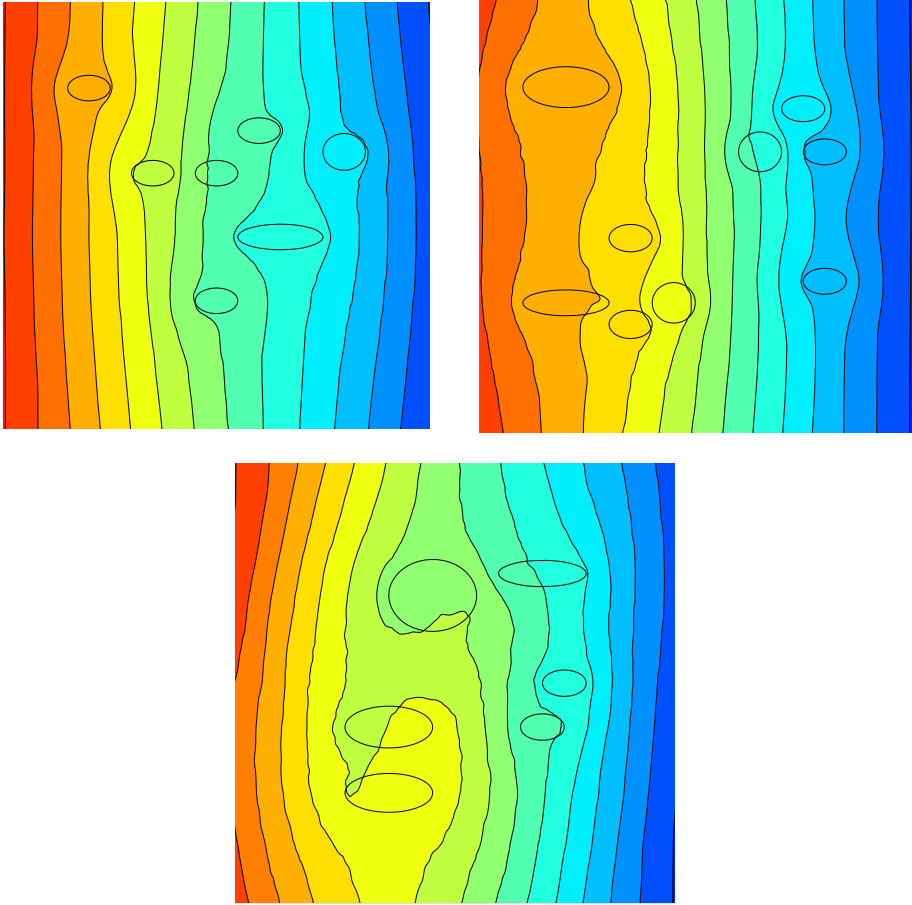


**Fig. 13** Example of pressure field for a random distribution of vugs

Using the pressure averaging approach for obtaining effective permeability as given in Eq. 70 for a spheroidal vug, one can use the pressure field that has already been obtained in the previous sections to determine the effective permeability. Note that in the spheroidal coordinate system, the volume integral is given as

$$\langle f \rangle = \int_0^{2\pi} \int_{-1}^1 \int_1^s f(s, t, \phi) c^3 (s^2 - t^2) ds dt d\phi, \tag{77}$$

and

$$\frac{\partial f}{\partial x} = \frac{\partial f}{\partial s} \frac{1}{ct} + \frac{\partial f}{\partial s} \frac{1}{cs}. \tag{78}$$

Figure 10 shows the normalized effective permeability of porous matrix including spherical and spheroidal vugs with various sizes. It can be seen that Maxwell method results in overestimating the effective permeability. Also, the effective permeability increases as the volume fraction of vugs increases. The elongated vugs result in more effective permeability, for the same volume fraction of vugs.

In Fig. 11, the effective permeability of a vuggy porous domain for a fixed-volume fraction of vugs is plotted vs. various numbers of vugs as well as for various aspect ratios. It can be seen that for the same volume fraction of vugs, the narrower the vugs are, the higher the effective permeability is. One vug enhances effective permeability more than several vugs with the same volume fraction, but the effect of the increase in number of vugs is not very significant. The small fluctuation in the results might be because of numerical error during calculating the volume integral.

The pressure field at the extents of the matrix domain is assumed to be uniform and unperturbed by the presence of the vugs; that is why the spatial position of the vugs has no significant effect on the effective permeability of the ensemble of domain.

The effective permeability of several cases of random distribution and various sizes of spheroidal vugs within a matrix medium is shown in Fig. 12. Overall, we can state that the parameter having the largest impact on the effective permeability is the volume fraction of the vugs. For a fixed-volume fraction, the less the number of vugs is, the higher the effective permeability will be. Examples of pressure field of some of the cases the authors considered are shown in Fig. 13.

## 6 Conclusions

The analytical solutions for the problem of the axis-symmetric flow of an incompressible fluid in a porous matrix including spherical and spheroidal vugs have been presented. Darcian flow in the matrix was coupled with Stokes flow in the vug through a no-jump condition of normal velocities, jump on pressures, and generalized Beavers–Joseph–Saffman condition, on the interface of the matrix and vug. The generalized form of the Beavers–Joseph–Saffman boundary condition allowed us to consider even very small sizes of vugs. The equivalent permeability of the vug was obtained by substituting it with a porous vug having the same external matrix pressure field. The developed solution reduces to the solution for spherical vugs when the focal length of the spheroid approaches zero.

In general, the equivalent permeability of the vug and the effective permeability of the entire domain are directly proportional to the volume fraction of the vug. The bigger the vugs volume is, the higher the effective permeability of the ensemble of the domain will be. For a fixed spheroidal major axis length, when the aspect ratio (the ratio of major spheroid axis to the minor spheroid axis) approaches one, the spheroid becomes a sphere, the volume fraction increases, and as a result, the equivalent permeability of the vug reaches its maximum. In contrary, for a given volume fraction, the minimum equivalent permeability is related to the minimum (unit) aspect ratio, that is when the vug becomes a sphere. The spatial position of the vugs has negligible effect on the effective permeability of the ensemble domain. Different spatial arrangement of one same set of vugs of various sizes does not change the effective permeability of the medium. This is a result of the regularization conditions at infinity that we imposed on the problem. For a fixed aspect ratio and same total vug volume fraction, increasing the number of vugs can reduce the effective permeability; however, the effect is not very significant. This is somehow a trivial result; a single big vug placed at the center of the porous domain enhances the effective permeability more compared to the case when the same vug volume is divided to smaller vugs spread out in the porous domain. The interaction of the streamlines through the passages between the vugs reduces a little bit the effective permeability. The difference is negligible.

**Acknowledgements** The authors are grateful to Schlumberger for permission to publish this article.



### Appendix 1: Gegenbauer Polynomials

The  $n$ th degree Gegenbauer polynomials of first and second kind and of degree  $-\frac{1}{2}$  are defined as

$$G_n(x) = \frac{1}{2n-1} (P_{n-2}(x) - P_n(x)), \tag{79}$$

$$G_0(x) = 1, \tag{80}$$

$$G_1(x) = -x, \tag{81}$$

$$H_n(x) = \frac{1}{2n-1} (Q_{n-2}(x) - Q_n(x)), \tag{82}$$

$$H_0(x) = -x, \tag{83}$$

$$H_1(x) = -1, \tag{84}$$

with the following properties

$$x^2 G_0(x) = G_0(x) - 2G_2(x), \tag{85a}$$

$$x^2 G_1(x) = G_1(x) + 2G_3(x), \tag{85b}$$

$$x^2 G_2(x) = \frac{1}{5} G_2(x) + \frac{4}{5} G_4(x), \tag{85c}$$

$$x^2 G_3(x) = \frac{3}{7} G_3(x) + \frac{4}{7} G_5(x), \tag{85d}$$

$$x^2 G_n(x) = \alpha_n G_{n-2}(x) + \gamma_n G_n(x) + \beta_n G_{n+2}(x), \tag{85e}$$

and

$$x^2 H_0(x) = x^2 G_1(x), \tag{86a}$$

$$x^2 H_1(x) = -x^2 G_0(x), \tag{86b}$$

$$x^2 H_2(x) = -\frac{1}{3} G_1(x) + \frac{1}{5} H_2(x) + \frac{4}{5} H_4(x), \tag{86c}$$

$$x^2 H_3(x) = \frac{1}{15} G_0(x) + \frac{3}{7} H_3(x) + \frac{4}{7} H_5(x), \tag{86d}$$

$$x^2 H_n(x) = \alpha_n H_{n-2}(x) + \gamma_n H_n(x) + \beta_n H_{n+2}(x), \tag{86e}$$

with

$$\alpha_n = \frac{(n-3)(n-2)}{(2n-3)(2n-1)}, \quad n \geq 4 \tag{87a}$$

$$\beta_n = \frac{(n+1)(n+2)}{(2n-1)(2n+1)}, \quad n \geq 4 \tag{87b}$$

$$\gamma_n = \frac{2n^2 - 2n - 3}{(2n+1)(2n-3)}, \quad n \geq 4. \tag{87c}$$

### Appendix 2: Series Expansion in Terms of the Legendre Polynomials

The orthogonality of the Legendre polynomials permits any function  $f(x)$  to be expressed in terms of a series in the basis of the Legendre polynomials  $P_n(x)$  as

$$f(x) = \sum_{n=0}^{\infty} a_n P_n(x), \tag{88}$$

with

$$a_n = \frac{2n + 1}{2} \int_{-1}^1 f(x) P_n(x) dx. \tag{89}$$

If  $f(x)$  is an even function, then the expansion includes only even terms; thus,

$$f(x) = \sum_{k=0}^{\infty} a_{2k} P_{2k}(x), \tag{90}$$

with

$$a_k = (4k + 1) \int_0^1 f(x) P_{2k}(x) dx. \tag{91}$$

### Appendix 3: Reduction to the Spherical Coordinate System

As it is shown in Fig. 14, when the semi-focal length  $c$  of the spheroidal coordinate system approaches zero, the coordinate system  $(\xi, \eta, \phi)$  reduces to a spherical coordinate system  $(\rho, \theta, \phi)$  where

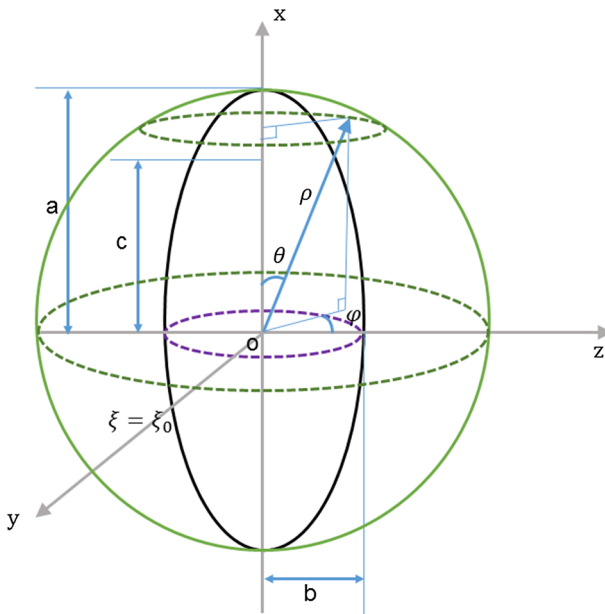


Fig. 14 Spheroidal coordinate and spherical coordinate systems

$$\rho = \sqrt{x^2 + y^2 + z^2} = \sqrt{s^2 + t^2 - 1}, \tag{92}$$

when  $c \rightarrow 0+$ , noting that  $s \geq 1$  and  $-1 \leq t \leq 1$ ; thus,

$$\lim_{c \rightarrow 0+} c s = \rho, \tag{93}$$

$$\lim_{c \rightarrow 0+} t = \cos \theta. \tag{94}$$

As a result, the term in the spheroidal coordinate system representing the radius is proportional to the radius in the spherical coordinate system.

It is possible to show that the results obtained in the spheroidal coordinate system can be converted to the actual results in the spherical coordinate if one replaces  $s$  by  $s/c$ , and then takes the limit of  $c^n G_n(s/c)$  and  $c^{1-n} H_n(s/c)$  as  $c \rightarrow 0+$  and then replaces  $s$  by  $r$ . We can show that

$$\lim_{c \rightarrow 0+} \frac{1}{2c} \ln \frac{x+1}{x-1} = \frac{1}{\rho}, \tag{95}$$

where we have used the expansion

$$\frac{1}{2} \ln \frac{x+1}{x-1} = \coth^{-1} x = \frac{1}{x} + \frac{1}{3x^3} + \frac{1}{5x^5} + \dots \tag{96}$$

The Gegenbauer polynomials have the equivalents when  $c \rightarrow 0+$  given by

$$\begin{aligned} c^0 G_0(s) &\rightarrow 1, & c G_1(s) &\rightarrow -\rho, \\ c^2 G_2(s) &\rightarrow -\frac{1}{2}\rho^2, & c^3 G_3(s) &\rightarrow -\frac{1}{2}\rho^3, \\ c^4 G_4(s) &\rightarrow -\frac{5}{8}\rho^4, & c^n G_n(s) &\rightarrow (\text{const})\rho^n, \quad n \geq 5, \end{aligned} \tag{97}$$

$$\begin{aligned} \frac{1}{c} H_2(s) &\rightarrow \frac{1}{3\rho}, & \frac{1}{c^2} H_3(s) &\rightarrow \frac{1}{15\rho^2}, \\ \frac{1}{c^3} H_4(s) &\rightarrow \frac{2}{105\rho^3}, & \frac{1}{c^{n-1}} H_n(s) &\rightarrow \frac{\text{const}}{\rho^{n-1}}, \quad n \geq 5. \end{aligned} \tag{98}$$

Prior to that, we have the following

$$\begin{aligned} c^n P_n(s) &\rightarrow (\text{const})\rho^n, \quad n \geq 0, \\ c^{-(n+1)} Q_n(s) &\rightarrow \frac{(\text{const})}{\rho^{n+1}}, \quad n \geq 0. \end{aligned} \tag{99}$$

## Appendix 4: Fluid Flow in the Matrix Medium Including a Spherical Vug

### Flow field in the matrix and in the spherical vug

For a spherical vug with a radius  $\rho = \rho_o$  located in the center of the porous domain of permeability  $k_m$ , the spherical coordinate system  $(\rho, \theta, \phi)$  with unit vectors  $(\mathbf{e}_\rho, \mathbf{e}_\theta, \mathbf{e}_\phi)$  is used. The scale factors for the spherical coordinate system are given as

$$h_1 = 1, \quad h_2 = \rho, \quad h_3 = \rho \sin \theta. \tag{100}$$

The solution to Stokes stream function that satisfies  $E^4 \Psi_s = 0$  in the spherical coordinate system together with the conditions in Eqs. 13 and 14 is given as

$$(\Psi_v)_s(\rho, \theta) = (B\rho^2 + C\rho^4) \sin^2 \theta, \quad \text{in } (\Omega_v)_s, \tag{101}$$

$$(u_v)_s(\rho, \theta) = 2(B + C\rho^2) \cos \theta, \quad \text{in } (\Omega_v)_s, \tag{102}$$

$$(v_v)_s(\rho, \theta) = -2(B + 2C\rho^2) \sin \theta, \quad \text{in } (\Omega_v)_s, \tag{103}$$

where we have used Eq. 9. The subscript “s” is used to point out that it is for a spherical vug. The pressure field can be determined by using Eq. 12 as

$$(p_v)_s(\rho, \theta) = 20C \mu \rho \cos \theta, \quad \text{in } (\Omega_v)_s. \tag{104}$$

Outside the spherical vug, the pressure field satisfies the Laplacian equation previously given in Eq. 3. This equation together with the condition of regularity of the pressure gradient at infinity (Eq. 15) gives the following determination for the matrix pressure as

$$(p_m)_s(\rho, \theta) = \left(\frac{D}{\rho^2} + |\nabla(p_m)_\infty|\rho\right) \cos \theta, \quad \text{in } (\Omega_m)_s. \tag{105}$$

Consequently, the velocity in the matrix domain is given as

$$\begin{aligned} (u_m)_s(\rho, \theta) &= \frac{k_m}{\mu} \left(2\frac{D}{\rho^3} - |\nabla(p_m)_\infty|\right) \cos \theta, \quad \text{in } (\Omega_m)_s, \\ (v_m)_s(\rho, \theta) &= \frac{k_m}{\mu} \left(\frac{D}{\rho^3} + |\nabla(p_m)_\infty|\right) \sin \theta, \quad \text{in } (\Omega_m)_s. \end{aligned} \tag{106}$$

Using Eq. 6, the stream function exterior to the vug can be written as

$$(\Psi_m)_s(\rho, \theta) = \left(\frac{k_m}{\mu} \frac{D}{\rho} + \frac{1}{2}U_\infty\rho^2\right) \sin^2 \theta, \quad \text{in } (\Omega_m)_s, \tag{107}$$

where  $U_\infty = -\frac{k_m}{\mu}|\nabla(p_m)_\infty|$ . The three sets of boundary conditions given in Eqs. 16, 17, and 20 are applied on the interface of the matrix and Stokes domain as

$$\begin{aligned} (u_v)_s &= (u_m)_s, \quad \text{on } \rho = \rho_o, \\ -(p_v)_s + 2\mu \frac{\partial(u_v)_s}{\partial\rho} &= -(p_m)_s, \quad \text{on } \rho = \rho_o, \\ \frac{\lambda}{\sqrt{k_m}}(v_v)_s &= \rho \frac{\partial}{\partial\rho} \left(\frac{(v_v)_s}{\rho}\right) + \frac{1}{\rho} \frac{\partial(u_v)_s}{\partial\theta}, \quad \text{on } \rho = \rho_o. \end{aligned} \tag{108}$$

Applying the boundary conditions of Eq. 108 to the velocity and pressure fields already obtained for the interior and exterior of the vug, which results in a system of three equations and three unknowns  $B, C, D$ , solvable as

$$C = \frac{\frac{3}{2} \frac{k_m}{\mu} \lambda |\nabla(p_m)_\infty|}{\lambda \rho_o^2 + 12\lambda k_m - 3\sqrt{k_m}\rho_o}, \tag{109}$$

$$B = C(3\sqrt{k_m} - 2\lambda\rho_o)\rho_o, \tag{110}$$

$$D = -|\nabla(p_m)_\infty|\rho_o^3 + \frac{18k_m\lambda|\nabla(p_m)_\infty|\rho_o^3}{\lambda\rho_o^2 + 12\lambda k_m - 3\sqrt{k_m}\rho_o}. \tag{111}$$

Instead of the generalized form of the Beavers–Joseph–Saffman boundary condition, Markov et al. (2010) have used the simplified form for the boundary condition expressed as

$$\frac{\lambda}{\sqrt{k_m}} v_s = \frac{\partial v_s}{\partial\rho}, \quad \text{on } \rho = \rho_o. \tag{112}$$

If one uses the simplified form of the Beavers–Joseph–Saffman boundary condition as in Eq. 112, then the matrix pressure field is different and is given as

$$D = -|\nabla(p_m)_\infty|\rho_o^3 + \frac{18k_m\lambda|\nabla(p_m)_\infty|\rho_o^3}{\lambda\rho_o^2 + 12\lambda k_m - 4\sqrt{k_m}\rho_o}. \tag{113}$$

**Equivalent Permeability of a Single Spherical Vug**

A porous spherical inclusion  $(\Omega_m)_{in,s}$  of radius  $\rho = \rho_o$  is located in the center of porous medium. The effective permeability of this porous inclusion  $(k_m)_{in,s}$  is chosen so that the pressure and flow field out of the inclusion stay the same as in the case of a fluid-filled vug. The pressure field inside the porous inclusion should satisfy the following equation

$$\nabla^2(p_m)_{in,s} = 0, \quad \text{in } (\Omega_m)_{in,s}, \tag{114}$$

where  $(p_m)_{in,s}$  represents the pressure in the porous inclusion. When considering the bounded pressure at the center of inclusion, the following applies

$$(p_m)_{in,s} = D_{in}\rho \cos \theta, \quad \text{in } (\Omega_m)_{in,s}. \tag{115}$$

This means that the first approximation of stream function inside the porous inclusion is a straight line which is a result of the use of Darcy’s law to describe the flow inside the inclusion. The boundary condition for coupling two porous domains inside and outside the inclusion is the no-jump boundary condition on the pressure and the normal fluxes on the interface as

$$(p_m)_s = (p_m)_{in,s}, \quad \text{on } \rho = \rho_o, \tag{116}$$

$$\frac{k_m}{\mu} \frac{\partial(p_m)_s}{\partial\rho} = \frac{(k_m)_{in,s}}{\mu} \frac{\partial(p_m)_{in,s}}{\partial\rho}, \quad \text{on } \rho = \rho_o, \tag{117}$$

where  $(p_m)_s$  is given in Eq. 105 and  $(k_m)_{in,s}$  is the effective permeability of equivalent spherical porous inclusion to be found. Solving the system of Eqs. 116 and 117 for  $\mathbb{D}$  and  $(k_m)_{in,s}$ , we obtain

$$(k_m)_{in,s} = k_m \left( 1 - \frac{3D}{(D + |\nabla(p_m)_\infty|\rho_o^3)} \right), \tag{118}$$

or

$$(k_m)_{in,s} = \frac{\rho_o^2}{6} \left( 1 - \frac{3\sqrt{k_m}}{\lambda\rho_o} \right). \tag{119}$$

Note that the simplified form of the Beavers–Joseph–Saffman boundary condition in Eq. 112 yields the effective permeability of the porous inclusion as

$$(k_m)_{in,s} = \frac{\rho_o^2}{6} \left( 1 - \frac{4\sqrt{k_m}}{\lambda\rho_o} \right). \tag{120}$$

**Appendix 5: Reduction in a Spheroidal Vug to Spherical Vug**

In this section, we investigate the behavior of the flow for the coupled Stokes flow and Darcy’s law in a vuggy porous medium with a spheroidal vug in the limit when the semi-focal length

of the spheroid approaches zero. This behavior is expected to comply with the results of the solution for the vuggy porous medium with a spherical vug presented in Appendix D.1.

*Stream Function Inside the Vug* Equation 47 gives the first approximation for the stream function inside the spheroidal vug. In the limit  $c \rightarrow 0+$ , and using Eqs. 93, 94, and 97, the stream function reduces to the same form as the stream function inside the spherical vug given in Eq. 101 as

$$\Psi_v(s, t) = \left( \underbrace{c^2 a_2 G_2(s)}_{\equiv -\frac{a_2}{2} \rho^2} + c^4 \underbrace{\left( \frac{\beta_2 C_2}{10} \right) G_4(s)}_{\equiv -\frac{C_2}{20} \rho^4} \right) \underbrace{G_2(t)}_{\equiv \frac{1}{2} \sin^2 \theta} . \tag{121}$$

which is

$$\Psi_v(\rho, \theta) = (\mathbb{B} \rho^2 + \mathbb{C} \rho^4) \sin^2 \theta, \tag{122}$$

with

$$\mathbb{B} = -\frac{a_2}{4}, \quad \mathbb{C} = \frac{-C_2}{40}. \tag{123}$$

*Pressure Field Inside the Vug* The first approximation for the pressure field inside the spheroidal vug is given in Eq. 49 as

$$p_v(s, t) = -\frac{1}{2} \mu c C_2 s t, \tag{124}$$

and when  $c \rightarrow 0+$ , using Eqs. 93 and 94, Eq. 124 reduces to

$$p_v(\rho, \theta) = 20 \mu \mathbb{C} \rho \cos \theta, \tag{125}$$

which is in accordance with the results obtained for the pressure inside the spherical vug given in Eq. 104.

*Pressure Field Outside the Vug* The first approximation for the pressure field outside the spheroidal vug in the matrix medium is given in Eq. 52 as

$$p_m(s, t) = c A_2 \left( \frac{1}{2} s \log \left( \frac{s+1}{s-1} \right) - 1 \right) t + c |\nabla(p_m)_\infty| s t, \tag{126}$$

when  $c \rightarrow 0+$ , and using Eqs. 93, 94, and 96, Eq. 126 reduces to the same form as the pressure outside the spherical vug given in Eq. 105, i.e.,

$$p_m(\rho, \theta) = \left( \frac{\mathbb{D}}{\rho^2} + |\nabla(p_m)_\infty| \rho \right) \cos \theta, \tag{127}$$

where

$$\mathbb{D} \equiv \frac{c^3 A_2}{3}. \tag{128}$$

*Stream Function Outside the Vug* The first approximation of the stream function outside the spheroidal vug is given in Eq. 56, and when  $c \rightarrow 0+$ , this equation reduces to

$$\Psi_m(s, t) = -c^2 \frac{k_m A_2}{\mu} \frac{A_2}{2} \sin^2 \theta \left( -\frac{2c}{3\rho} - \frac{c^3}{3\rho^3} \right) - \frac{1}{2} \frac{k_m}{\mu} c^2 |\nabla(p_m)_\infty| \frac{\rho^2 - c^2}{c^2} \sin^2 \theta. \tag{129}$$

This equation is equivalent to the stream function external to the spherical vug given in Eq. 107, i.e.,

$$\Psi_m(s, t) = \frac{k_m}{\mu} \left( \frac{\mathbb{D}}{\rho} - \frac{1}{2} |\nabla(p_m)_\infty| \rho^2 \right) \sin^2 \theta. \tag{130}$$

## References

- Aarseth, E.S., Bourgine, B., Castaing, C., Chiles, J.R., Christensen, N.R., Eeles, M., Fillion, E., Genter, A., Gillespie, R.A., Hakansson, E., Jorgensen, K.Z., Lindgaard, H.F., Madsen, L., Odling, N.E., Olsen, C., Reffstrup, J., Trice, R., Walsh, J.J., Watterson, J.: Interim guide to fracture interpretation and flow modeling in fractured reservoirs. Technical report EUR 17116 EN, European Commission (1997)
- Arbogast, T., Brunson, D.S.: A computational method for approximating a Darcy–Stokes system governing a vuggy porous medium. *Comput. Geosci.* **11**(3), 207–218 (2007)
- Arbogast, T.D., Brunson, S.B., Jennings, J.: A preliminary computational investigation of a macro-model for vuggy porous media. In: Miller, C.T., Farthing, M.W., Gray, W.G., Pinder, G.F. (eds.), *Computational Methods in Water Resources: Volume 1, volume 55, Part 1 of Developments in Water Science*, pp. 267–278. Elsevier, Chapel Hill (2004)
- Arbogast, T., Gomez, M.S.M.: A discretization and multigrid solver for a Darcy–Stokes system of three dimensional vuggy porous media. *Comput. Geosci.* **13**(3), 331–348 (2009)
- Arbogast, T., Lehr, H.L.: Homogenization of a Darcy–Stokes system modeling vuggy porous media. *Comput. Geosci.* **10**(3), 291–302 (2006)
- Arns, C., Bauget, F., Limaye, A., Sakellariou, A., Senden, T., Sheppard, A., Sok, R., Pinczewski, W., Bakke, S., Berge, L., Oren, P., Knackstedt, M.: Pore-scale characterization of carbonates using X-ray microtomography. *SPE J.* **10**(4), 475–484 (2005)
- Beavers, G.S., Joseph, D.D.: Boundary conditions at a naturally permeable wall. *J. Fluid Mech.* **30**, 197–207 (1967)
- Belfield, W., Sovich, J.: Fracture statistics from horizontal wellbores. In: Paper HWC-94-37, SPE/CIM/CANMET International Conference on Recent Advances in Horizontal Well Applications, March 20–23, Calgary, Canada (1994)
- Bertels, S.P., DiCarlo, D.A., Blunt, M.J.: Measurement of aperture distribution, capillary pressure, relative permeability, and in situ saturation in a rock fracture using computed tomography scanning. *Water Resour. Res.* **37**(3), 649–662 (2001)
- Bouchelaghem, F.: Flow study in a double porosity medium containing ellipsoidal occluded macro-voids. *Math. Geosci.* **43**(1), 55–73 (2011a)
- Bouchelaghem, F.: Flow study in a double porosity medium containing low concentrations of ellipsoidal occluded macro-voids. *Math. Geosci.* **43**(1), 23–53 (2011b)
- Braester, C.: Groundwater flow through fractured rocks, pp. 22–42. In: Luis S., Usunoff E.J. (eds.) *GROUNDWATER—Vol. II, EOLSS/ UNESCO, 1st edn* (2005)
- Bruggeman, D.A.G.: Berechnung verschiedener physikalischer konstanten von heterogenen substanzen. i. dielektrizitätskonstanten und leitfähigkeiten der mischkörper aus isotropen substanzen. *Annalen der Physik* **416**(7), 636–664 (1935)
- Charalambopoulos, A., Dassios, G.: Complete decomposition of axisymmetric Stokes flow. *Int. J. Eng. Sci.* **40**(10), 1099–1111 (2002)
- Committee on Fracture Characterization and Fluid Flow: *Rock Fractures and Fluid Flow: Contemporary Understanding and Applications*. The National Academies Press, Washington, DC (1996)
- Dassios, G.: The fundamental solutions for irrotational and rotational Stokes flow in spheroidal geometry. *Math. Proc. Camb. Philos. Soc.* **143**, 243–253 (2007)
- Dassios, G., Hadjinicolaou, M., Payatakes, A. C.: Generalized eigenfunctions and complete semiseparable solutions for Stokes flow in spheroidal coordinates. *Q. Appl. Math.* **LII**(1), 157–191 (1994)
- Dassios, G., Payatakes, A.C., Vafeas, P.: Interrelation between Papkovitch–Neuber and Stokes general solutions of the Stokes equations in spheroidal geometry. *Q. J. Mech. Appl. Math.* **57**(2), 181–203 (2004)
- Detwiler, R.L., Rajaram, H., Glass, R.J.: Nonaqueous-phase-liquid dissolution in variable-aperture fractures: development of a depth-averaged computational model with comparison to a physical experiment. *Water Resour. Res.* **37**(12), 3115–3129 (2001)
- Fitts, C.R.: Modeling three-dimensional flow about ellipsoidal inhomogeneities with application to flow to a gravel-packed well and flow through lens-shaped inhomogeneities. *Water Resour. Res.* **27**(5), 815–824 (1991)
- Happel, J., Brenner, H.: *Low Reynolds Number Hydrodynamics: With Special Applications to Particulate Media. Mechanics of Fluids and Transport Processes*. Springer, Berlin (1983)
- Iyengar, T., Radhika, T.: Stokes flow of an incompressible micropolar fluid past a porous spheroidal shell. *Bull. Pol. Acad. Sci. Tech. Sci.* **59**(1), 63–74 (2011)
- Iyengar, T., Radhika, T.: Couple stress fluid past a porous spheroidal shell with solid core under Stokesian approximation. *J. Sci. Res. Rep.* **6**(1), 43–60 (2015)
- Jones, I.P.: Low Reynolds number flow past a porous spherical shell. *Math. Proc. Camb. Philos. Soc.* **73**, 231–238 (1973)

- Keller, A.A., Roberts, P.V., Blunt, M.J.: Effect of fracture aperture variations on the dispersion of contaminants. *Water Resour. Res.* **35**(1), 55–63 (1999)
- Kuchuk, F., Biryukov, D., Fitzpatrick, T.: Fractured-reservoir modeling and interpretation. *SPE J.* **20**(04) 983–1004 (2015)
- Lucia, F.J.: *Carbonate Reservoir Characterization*. Environmental Science. Springer, Berlin (1999)
- Markov, M., Kazatchenko, E., Mousatov, A., Pervago, E.: Permeability of the fluid-filled inclusions in porous media. *Transp. Porous Media* **84**(2), 307–317 (2010)
- Moctezuma-Berthier, A., Vizika, O., Adler, P.: Macroscopic conductivity of vugular porous media. *Transp. Porous Media* **49**(3), 313–332 (2002)
- Moctezuma-Berthier, A., Vizika, O., Thovert, J.F., Adler, P.: One- and two-phase permeabilities of vugular porous media. *Transp. Porous Media* **56**(2), 225–244 (2004)
- Nurmi, R., Kuchuk, F., Cassell, B., Chardac, J.-L., Maguet, L.: Horizontal highlights. Schlumberger Middle East Well Eval. *Rev.* **16**, 6–25 (1995). [http://www.slb.com/~media/Files/resources/mearr/wer16/rel\\_pub\\_mewer16\\_1.pdf](http://www.slb.com/~media/Files/resources/mearr/wer16/rel_pub_mewer16_1.pdf)
- Popov, P., Efendiev, Y., Qin, G.: Multiscale modeling and simulations of flows in naturally fractured karst reservoirs. *Commun. Comput. Phys.* **6**(1), 162 (2009)
- Radhika, T.S.L., Iyengar, T.: Stokes flow of an incompressible couple stress fluid past a porous spheroidal shell. In: *Proceedings of the International MultiConference of Engineers and Computer Scientists*, volume III (2010)
- Raja Sekhar, G., Sano, O.: Viscous flow past a circular/spherical void in porous media—an application to measurement of the velocity of groundwater by the single boring method. *J. Phys. Soc. Jpn.* **69**(8), 2479–2484 (2000)
- Raja Sekhar, G., Sano, O.: Two-dimensional viscous flow in a granular material with a void of arbitrary shape. *Phys. Fluids* **15**, 554–567 (2003)
- Rubin, Y., Gómez-Hernández, J.J.: A stochastic approach to the problem of upscaling of conductivity in disordered media: theory and unconditional numerical simulations. *Water Resour. Res.* **26**(4), 691–701 (1990)
- Saffman, P.G.: On the boundary condition at the surface of a porous medium. *Stud. Appl. Math.* **50**(2), 93–101 (1971)
- Wieck, J., Person, M., Strayer, L.: A finite element method for simulating fault block motion and hydrothermal fluid flow within rifting basins. *Water Resour. Res.* **31**(12), 3241–3258 (1995)
- Zhao, C., Valliappan, S.: Numerical modelling of transient contaminant migration problems in infinite porous fractured media using finite/infinite element technique. Part II: parametric study. *Int. J. Numer. Anal. Methods Geomech.* **18**(8), 543–564 (1994)